Coaly and lacustrine hydrocarbon source rocks in Permo-Carboniferous graben deposits (Weiach well, Northern Switzerland)

Stephen Ajuaba, Reinhard F. Sachsenhofer, Verena Meier, Doris Gross, Johann Schnyder, Silvia Omodeo-Salé, Andrea Moscariello, David Misch

Marine and Petroleum Geology 150 (2023) 106147

Contents lists available at ScienceDirect

Marine and Petroleum Geology

journal homepage: www.elsevier.com/locate/marpetgeo

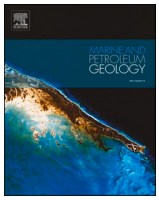

Coaly and lacustrine hydrocarbon source rocks in Permo-Carboniferous graben deposits (Weiach well, Northern Switzerland)

Stephen Ajuaba [a,*], Reinhard F. Sachsenhofer [a], Verena Meier [a,b], Doris Gross [a], Johann Schnyder [c], Silvia Omodeo-Salé [d], Andrea Moscariello [d], David Misch [a]

[a] Lehrstuhl Erdölgeologie, Montanuniversitaet Leoben, Peter-Tunner-Strasse 5, 8700, Leoben, Austria
[b] Institute of Hydrogeology, Engineering Geology and Applied Geophysics, Charles Univesity Prague, Czech Republic
[c] Sorbonne Université, CNRS-INSU, Institut des Sciences de La Terre de Paris, ISTeP, 4 Place Jussieu, 75005, Paris, France
[d] Department of Earth Sciences, University of Geneva, Switzerland

ARTICLE INFO

Keywords:
Permo-Carboniferous sediments
Permian lacustrine shales
Carboniferous coals
Hydrocarbon potential
Gas potential
Palynofacies
Anoxic lake
Stratified water column

ABSTRACT

Permo-Carboniferous graben sediments in the North Alpine Foreland Basin (NAFB) include Upper Carboniferous (Stephanian) coal-measures and lower Permian (lower Autunian) lacustrine shales with high organic matter contents. Coals are probably the source for a gas accumulation in Switzerland, while the bituminous shales are potential source rocks for oil. In order to study the hydrocarbon potential of coal and bituminous shales and to contribute to the understanding of their depositional environment, 90 core samples from the Weiach-1 well (northern Switzerland) were investigated using organic petrographic, palynofacies, Rock-Eval pyrolysis, and geochemical techniques (incl. biomarker analysis and compound-specific carbon isotopy). Carboniferous coal seams are up to 10 m thick and were deposited in low-lying freshwater mires. They contain a significant gas potential and reached a maturity stage related to the onset of gas generation. Sapropelic rocks were not observed in the coal-bearing succession. Organic matter-rich Permian shales (Autunian shales) were deposited in anoxic lakes with a stratified water column. The organic matter is of mixed aquatic and terrigenous origin. $\delta^{13}C$ values of chlorophyll-derived isoprenoids provide evidence for reworking of organic matter in the water column. The Autunian shales have a strongly varying, but locally very good oil potential. They reached early oil window maturity, but did not yet generate significant amounts of hydrocarbons. The main shale interval in the studied borehole is about 12 m thick and will generate about 0.35 tHC/m^2 when mature. A comparison with literature data shows that it is possible to distinguish oils generated from Permian, Jurassic and Oligocene source rocks based on biomarker ratios and isotope data.

1. Introduction

Post-Variscan tectonics resulted in the formation of a series of Permo-Carboniferous strike-slip and extensional basins in central and western Europe (e.g., McCann et al., 2006). Many of these basins are filled with latest Carboniferous coal-bearing sediments and early Permian lacustrine deposits (McCann et al., 2006; Mercuzot et al., 2022). Elongated Permo-Carboniferous coal-bearing basins are also present in the basement of the North Alpine Foreland Basin (NAFB; Fig. 1) (e.g., Bachmann et al., 1987; Madritsch et al., 2018).

The extension and sedimentary infill of the Permo-Carboniferous grabens are poorly known. This is because high resolution seismic data illuminating the grabens are scarce and only very few wells penetrated the graben deposits. The most intensively studied graben structure is named the Constance-Frick Trough and is located in northern Switzerland (Diebold et al., 1991; Laubscher, 1987; Madritsch et al., 2018; Moscariello et al., 2021). At present, the Constance-Frick Trough is buried beneath Cenozoic and Mesozoic sediments, more than 1 km thick. Only few wells have reached the Permian and Carboniferous sediments in the Constance-Frick Trough and only the Weiach-1 well, drilled by NAGRA (National Cooperative for the Disposal of Radioactive Waste) in 1983, has crossed the entire Permo-Carboniferous succession. With a total depth of 2482 m, this well penetrates Cenozoic Molasse sediments, Mesozoic sediments and the entire Permo-Carboniferous succession down to the crystalline basement (Fig. 2).

In the past century, the Constance-Frick area has been the object of

* Corresponding author.
E-mail address: stephen.ajuaba@unileoben.ac.at (S. Ajuaba).

https://doi.org/10.1016/j.marpetgeo.2023.106147
Received 3 November 2022; Received in revised form 7 December 2022; Accepted 28 January 2023
Available online 2 February 2023

different exploration activities, triggered by the economic interest in potential resources in the Carboniferous and Permian deposits, first by the coal mining industry and afterwards by the oil and gas industry (Diebold et al., 1991; Thury et al., 1994; Lahusen and Wyss, 1995; Greber et al., 1997). Currently, there is renewed interest in the area thanks to the development of deep geothermal and CO_2 storage projects that envisage new targets in these deposits (Swiss Office of Energy; Energy strategy 2050).

The NAFB contains a number of hydrocarbon deposits in its eastern (Austrian) and central (German) sectors. In addition, shallow hydrocarbon indications are present along the entire NAFB, and are especially abundant in the western (Swiss) sector (Misch et al., 2017). The main source rocks for oil and gas in the NAFB are the lower Oligocene Schöneck Formation and the Lower Jurassic Posidonia Shale (Wehner and Kuckelkorn, 1995; Schulz et al., 2002; Veron, 2005; Gratzer et al., 2011; Bechtel et al., 2019). In the Swiss western part, Carboniferous coal is probably the source rock of the Entlebuch gas field (for location see Fig. 1; Vollmayr and Wendt, 1987; Leu, 2012) and gas encountered by the St. Gallen GT-1 geothermal well (Omodeo-Salé et al., 2020). Permian lacustrine shales, together with the Toarcian Posidonia black shales, have been discussed as potential source rock for oil in the western part of the NAFB (Schegg and Leu, 1998; Veron, 2005; Leu, 2014; Misch et al., 2017; Moscariello, 2019; Do Couto et al., 2021) including the Jura Mountains (Pullan and Berry, 2019).

Hydrocarbon occurrence and migration at shallow and deep depths can represent a serious risk for the geothermal exploration activity and for the nuclear waste storage (Moscariello, 2019; Moscariello et al., 2020; Omodeo-Salé et al., 2020 and reference herein related to the St. Gallen incident while drilling a deep geothermal well). Therefore, to assess the type and the amount of hydrocarbons that can be generated at various depths is essential to properly evaluate this risk.

The hydrocarbon potential of the Permo-Carboniferous deposits in Switzerland is poorly known, based on few published data on their maturity and organic carbon content (Matter, 1987; Leu et al., 2001; NAGRA, 2002; Omodeo-Salé et al., 2020). The main goal of this study is to characterize coaly and shaly rocks, from the Weiach-1 well core material, using a wide array of techniques, including bulk geochemical data, organic petrology, biomarker, and compound-specific isotope data. Apart from a realistic assessment of the hydrocarbon potential, the study will also provide a basis for future oil to source correlation.

2. Geological setting

The Late Carboniferous consolidation of the Variscan orogen was followed by latest Carboniferous (Stephanian) to early Permian wrench-induced collapse (Ziegler et al., 2006). Across Europe, Permo-Carboniferous graben structures resulted from the post-Variscan transtensional activity (McCann et al., 2006). In Switzerland, several Permo-Carboniferous grabens have been recognized, segmenting the crystalline basement of the NAFB (Madritsch et al., 2018; Diebold et al., 1991; Leu, 2008). One of the most extended and best studied grabens is the Constance-Frick-Trough, extending along the northern rim of the NAFB (Laubscher, 1987; Diebold, 1988; Diebold et al., 1991; McCann et al., 2006, Fig. 1b).

A detailed description of the architecture and evolution of the Constance-Frick Trough (CFT) was provided by Madritsch et al. (2018). According to these authors, the 10–12 km wide CFT consists of two segments probably with opposing half-graben geometries, the eastern Weiach segment and the deeper western Riniken segment. The basin fill was subdivided into a lower, middle, and upper trough fill, which correspond to the Upper Carboniferous, Lower and Upper Permian clastic successions, respectively (Matter, 1987; Madritsch et al., 2018).

The Constance-Frick Trough was penetrated by two wells: Weiach-1 (Matter, 1987; Matter et al., 1988; Moscariello et al., 2021) and Riniken-1 (Matter et al., 1988). The 2482-m-deep Weiach-1 well penetrates the entire Permo-Carboniferous stratigraphic record (Matter, 1987; Matter et al., 1988; Moscariello et al., 2021). In contrast, the Riniken-1 well, drilled to a depth of 1618 m, only penetrated the

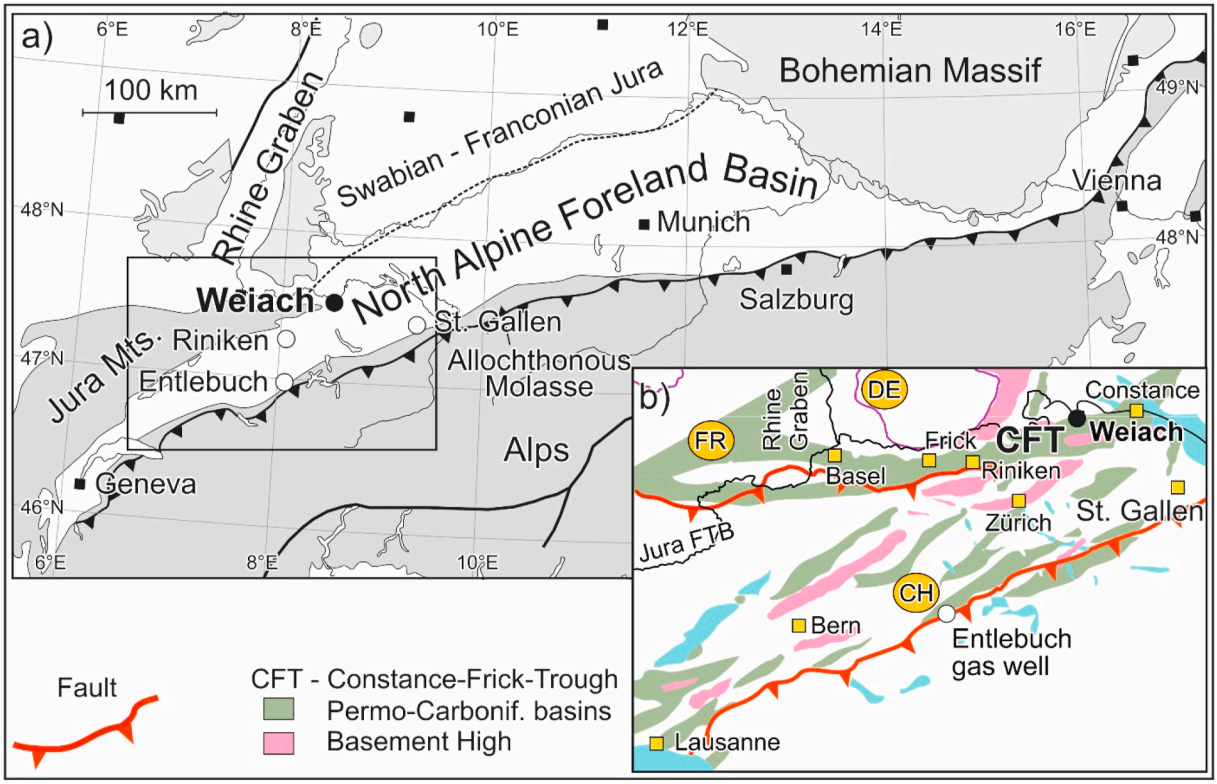

Fig. 1. a) Sketch map of the North Alpine Foreland Basin (NAFB) with location of the Weiach-1, Riniken-1 and St. Gallen wells, and the Entlebuch gas field in Switzerland, b) Distribution of Permo-Carboniferous graben structure in the basement of the NAFB (after Madritsch et al., 2018). CFT - Constance-Frick Trough.

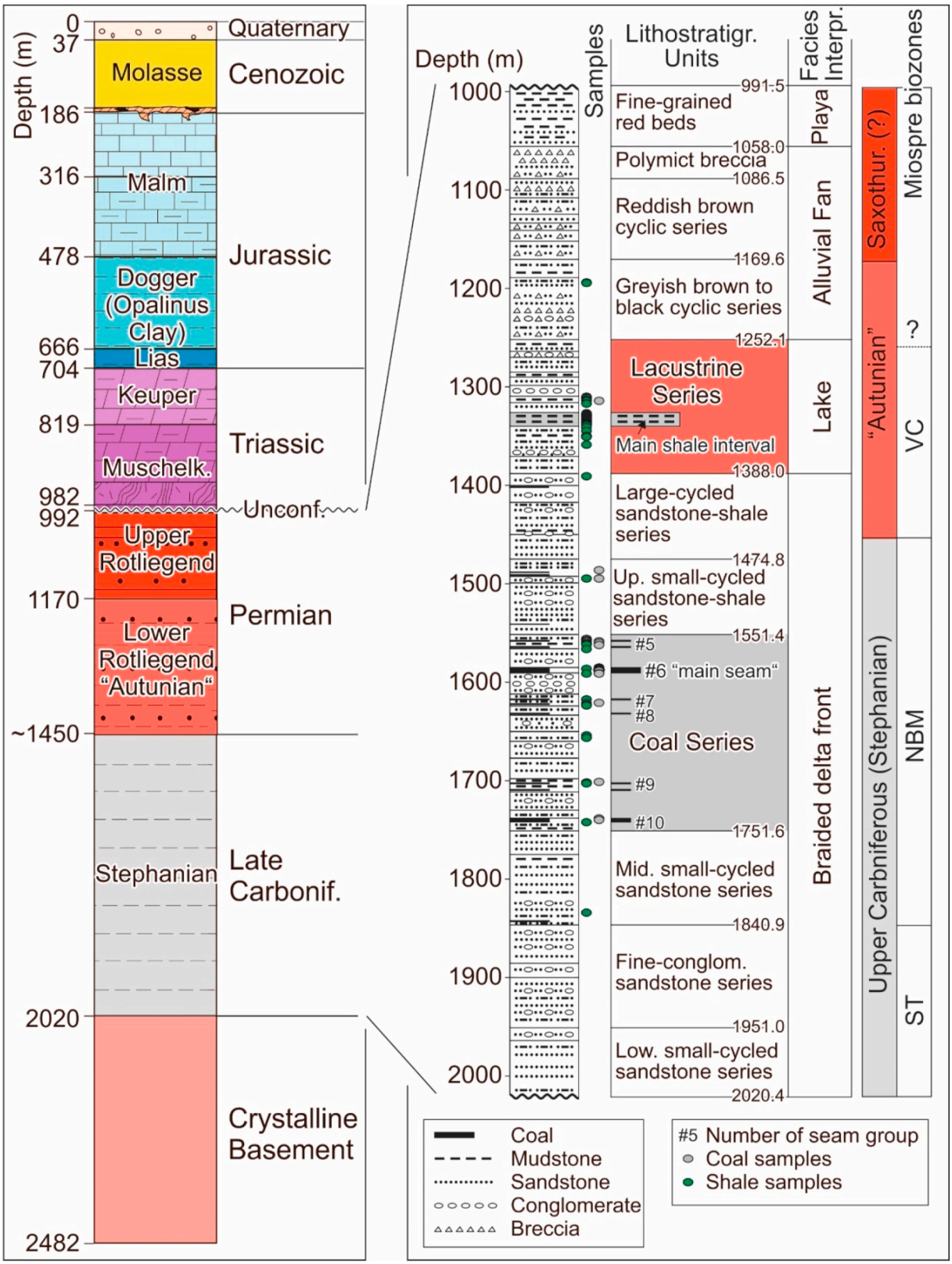

Fig. 2. Stratigraphy of the Weiach-1 borehole (modified after Matter et al., 1988 and Moscariello et al., 2021). The position of shale and coal samples is shown. Subdivision into biozones follows Hochuli (1985). ST – *Angulisporites splendidus-Latensina trilete* zone; NBM - *Potonieisporites novicus-bhardwajii-Cheiledonites major* zone; VC - *Vittatina costabilis* zone.

coarse-grained upper Permian unit.

This study focuses on the Weiach-1 well. A lithostratigraphic sketch of the well is show in Fig. 2. The Permo-Carboniferous succession in this well starts with coarse-grained sediments (2020-1388 m) was originally interpreted as an anastomosing fluvial system. Recently, a detailed sedimentological study of the same sequence (Cervelli, 2022; Moscariello et al., 2021) indicated dominant deposition associated with a braided delta front prograding periodically into a relatively deep (below wave base) lacustrine environment. This stratigraphic interval has been subdivided into six lithostratigraphic units and includes a Coal Series between 1752 and 1551 m (Fig. 2). Based on palynological data, Hochuli (1985) dated the main part of fluvial succession as Stephanian (*Angulisporites spledidus-Latensina trilete* [ST] and *Potonieisporites novicus-bhardwajii-Cheiledonites major* [NBM] zones; Clayton et al. (1977). The boundary to the early "Autunian" *Vittatina costabilis* [VC] zone (Carboniferous/Permian boundary) is within the interval from 1443.0 to 1451.5 m. The fluvial deposits are overlain by lacustrine sediments (Autunian Lacustrine Series; 1388-1252 m). The upper part of the Permian succession was deposited in alluvial fan and playa lake environments and is characterized by red colours. Mesozoic sediments follow above a major unconformity.

The Coal Series comprises nine fining-upward cycles, which include coarse gravels and sandstones, six groups of coal seams (from bottom to top #10 to #4, according to Matter et al., 1988, Fig. 2) and laminated shale. The main coal seam (#6; 1585.01–1591.23 m) is about 6 m thick. The laminated shale has been described as bituminous (e.g. Matter, 1987; Diebold, 1988). The depositional environment of the Coals Series was originally interpreted as belonging to a flood plain (Matter, 1987; Matter et al., 1988) whereas more recent investigation revealed the occurrence of several indicators of reworking processes associated with subacqueous sedimentary facies (i.e. slumps, sedimentary gravity flows) suggesting the likely resedimentation of the coal units in a delta front environment (Moscariello et al., 2021).

The Autunian Lacustrine Series (1388-1252 m) overlies the delta front sediments. The following description is based on Matter et al. (1988). The sedimentologically highly variable series is characterized by frequent facies changes, resulting from rapid shifting of the facies areas in the lakeshore area. It includes debris-flow conglomerates, fining-upward cycles, turbiditic graded siltstone rhythmites, black shales and stromatolithic layers. Matter et al. (1988) describe two "megacycles" which start with fluvial to deltaic channel sands and grade into lacustrine shales. The lacustrine shales often contain fish scales and ostracodes, indicating oxygen-rich water. In contrast, the laminated bituminous shales contain very high amounts of organic matter proving oxygen-deficient or even anoxic conditions (Matter, 1987). Probably the lake sediments were deposited in a complex and extensive early Permian lakescape (Matter, 1987).

Grey and subsequently red coarse-grained clastic sediments representing alluvial fans follow above the lacustrine deposits (1252.07–1058.03 m). Fine-grained red-coloured playa sediments (1058.03–991.50 m) are the youngest Permian deposits preserved (Diebold, 1988).

Random vitrinite reflectance (%Rr) data of the Weiach-1 well was provided by Leu et al. (2001) and NAGRA (2002). Vitrinite reflectance increases from ~0.7 %Rr at the top of the Permo-Carboniferous succession to ~1.25 %Rr at 1950 m depth. Mazurek et al. (2006), Leu (2012) and Omodeo-Salé et al. (2021) used these reflectance data to calibrate the heat flow history of the Weiach area. Based on these models, it is likely that Permian heat flow was high (125 mW/m^2; Omodeo-Salé et al., 2021) and that gas generation from Permo-Carboniferous coals occurred already during Permian time (Leu, 2012).

Based on the palynological data of Hochuli (1985), the Coal Series (late Stephanian NBM zone) and the Lacustrine Series (early "Autunian" VC zone) can be correlated with the Igornay Formation and the Muse Formation in the Autun Basin, respectively (Mercuzot et al., 2022).

3. Samples and analytical methods

3.1. Sampling

The present study is based on 90 core samples from the Weiach-1 well, taken with the permission of SwissTopo at the core shed of NAGRA in Hochdorf in the frame of the UNCONGEO project (University of Geneva). The samples were collected in the Carboniferous (Stephanian) Coal Series (22 shale and 22 coal samples) and the Permian ("Autunian") Lacustrine Series (46 shales samples; Fig. 2).

Samples were taken from different coal seams and shale intervals to provide information on stratigraphic variations. In order to study variations at high resolution, 13 coal samples were taken from the 5-m-thick "main seam #6" (1585.0–1591.2 m; Wolf et al., 1988; see Fig. 2), which is the most important seam in the succession, and 25 samples were taken from the thickest black shale interval in the Lacustrine Series (1326.9–1338.4 m), which is termed the main shale interval in this paper (Fig. 2).

Bulk parameters were determined for all samples. A sample subset was selected for organic petrographic, biomarker, and isotope investigations. This subset includes six coal samples from the main seam #6 together with a sample from underlying shale and 21 samples from the Permian Lacustrine Series. The latter samples cover all organic matter-rich shale intervals with a special focus on the main shale interval (13 samples).

3.2. Analytical methods

With the exception of palynological investigations, the analytical work was performed at the laboratories of the Chair Petroleum Geology at Montanuniversitaet Leoben (Austria). Palynological preparations were made at the iSTEP laboratory from Sorbonne Université, Paris (France).

3.2.1. Bulk parameters

All samples were analyzed for total carbon (TC; %), total sulphur (TS; %) and total organic carbon (TOC; %) using an Eltra Helios CS elemental analyzer. Samples pre-treated with concentrated phosphoric acid were used for the TOC measurements. The difference between TC and TOC was used to calculate calcite equivalent percentages ($calcite_{equiv.}$ = 8.334*(TOC-TIC).

Rock-Eval parameters (S_1, S_2 [mgHC/g rock]; T_{max} [°C]) were determined using a "Rock-Eval 6" instrument. S_1 and S_2 peaks are hydrocarbons volatized at 300 °C and hydrocarbons pyrolyzed from kerogen during gradual heating from 300 to 650 °C, respectively. T_{max} is the temperature of maximum S_2 hydrocarbon generation and serves as a maturity indicator. The hydrogen index (HI = 100 × S_2/TOC), the production index (PI = S_1/[S_1+S_2]) and the petroleum potential (PP = S1+S2) were calculated (Espitalie et al., 1977). A bitumen index (BI = 100xS_1/TOC) and a quality index (QI = 100x(S_1+S_2)/TOC) were calculated for coal samples (Sykes and Snowdon, 2002).

3.2.2. Organic petrography

Organic petrographic investigations were performed using a Leica DM 4P microscope with a 50× oil immersion objective. Semi-quantitative macerals analysis was carried out in white and fluorescence light using a single scan method. Approximately 1500 and 550 points were counted for the shale and coal samples, respectively. The results were normalized to 100% organic matter. The maceral terminology used follows the ICCP system (ICCP, 1998, 2001; Pickel et al., 2017), with the exception that fusinite is subdivided into pyro- and degradofusinite. Random vitrinite reflectance (%Rr) of four shale and two coal samples was determined in non-polarized light with a wavelength of 546 nm (Taylor et al., 1998). At least 50 particles were measured for shale samples and 100 particles for coals. The microscope was calibrated with a synthetic reflectance standard (N-LASF46A; Rr:

1.311%).

3.2.3. Palynofacies

The palynofacies approach allows the assessment of the origin and preservation state of particulate organic matter in sedimentary deposits (e.g., Steffen and Gorin, 1993; Tyson, 1995; McArthur et al., 2016; Schnyder et al., 2017). Twelve bulk samples from the Permian main shale interval (1326.9–1338.4 m) were selected and treated at the iSTEP laboratory from Sorbonne Université, Paris, France by HCl–HF using the standard procedure of Steffen and Gorin (1993). The resulting organic residues were used to make a first set of non-filtered slides. An aliquot of each sample was also filtered with a 10 μm sieve mesh and the >10 μm fraction was used to prepare a second set of filtered slides. Qualitative palynofacies observations were performed on all slides using an Axioplan2 Imaging Zeiss microscope in transmitted light. The filtered slides only were used for quantitative observations. For each filtered slide, at least 30 fields were counted yielding more than 500 particles, the threshold considered to be relevant to obtain a statistically valid count (Tyson, 1995). In this study, continental particles correspond to opaque and translucent vascular plant fragments, to a palynomorph group consisting of spores and pollen grains, and to rare occurrences of *Botryococcus*, a colonial algae indicative of freshwater to brackish water masses (e.g Tyson, 1995). Some hyphae from fungi are also observed. Amorphous organic matter (AOM) has also been observed. It correspond to orange to dark brown or even grey flakes, the origin of which cannot be determined at the microscopic scale. AOM is generally considered as deriving from algal/bacterial phytoplankton, although a higher plant tissue origin has also been proposed in some cases (Burdige, 2007; Tyson, 1995).

3.2.4. Biomarker analysis

Solvent extraction of powdered shale (5–10 g) and coal material (~1.5 g) was performed for ~1 h on a Dionex ASE 350 instrument using dichloromethane at 75 °C and 100 bar. A Zymark TurboVap 500 closed cell concentrator was used to concentrate the extract to ~0.5 ml. This was followed by asphaltene precipitation using a hexane:dichloromethane solution (80:1, v/v) and separation using centrifugation. The hexane-soluble fractions were further separated into polar fractions (NSO compounds), saturated and aromatic hydrocarbons using a Köhnen-Willsch MPLC (medium pressure liquid chromatography) instrument (Radke et al., 1980). Before the GC-MS measurement, equivalent amounts of internal standards (squalane for aliphatics; 1, 1′-binaphthyl for aromatics) were added to each sample.

The saturated hydrocarbon fractions were analyzed for *n*-alkanes and isoprenoids by a gas chromatograph (Trace GC-Ultra) attached to a flame ionization detector (GC-FID), equipped with a 50 m HP-PONA capillary column (inner diameter [i.d.] 0.20 mm, 0.50 μm film thickness). The sample was injected splitless at 270 °C, and oven temperature increased from 70 to 310 °C followed by 35 min isothermal period.

Analysis of specific biomarker molecules in the saturated and aromatic fractions was performed using gas chromatography-mass spectrometry (GC-MS) by a Thermo Scientific Trace GC-Ultra installed with a 60 m TG/DB-5MS fused silica capillary column (i.d. 0.25 mm; 0.25 μm film thickness) coupled to ThermoFisher ISQ mass spectrometer. The oven temperature was initially programed from 40 °C/min, held for 2 min and raised up to 310 °C with 4 °C/min followed by an isothermal period of 40 min. The sample was injected in split mode with a split ratio of 20 at 260 °C using helium as carrier gas. The spectrometer was operated in the EI (electron ionization) mode with a mass-to-charge ratio (*m/z*) scan range from *m/z* 50 to *m/z* 650 (0.7 s total scan time). Xcalibur and Chromeleon data systems were used for data processing. Identification of individual compounds was based on their respective retention time within the mass spectra or total ion current (TIC) chromatogram and comparing the mass spectra with published data as reference. From the distinct compound groups in the aliphatic and aromatic fraction, absolute concentrations were determined using peak areas in the TIC chromatograms comparable to that of internal standards while in the case of mass chromatograms, response factor were used to correct the intensities of the fragment ions used for quantification of the total ion abundance per sample. The sample concentrations were standardized to their respective TOC.

3.2.5. Compound-specific carbon isotopy

For the analysis of stable carbon isotope ratios on individual *n*-alkanes and isoprenoids, the *n*-alkanes were separated from the *iso*-alkanes within the saturated hydrocarbon fraction by an improved 5 Å molecular sieve method (Grice et al., 2008). Isotope analysis was performed using a Trace GC-Ultra gas chromatograph attached to the ThermoFisher Delta-V isotope ratio mass spectrometer (IRMS) via a combustion and high temperature reduction interface (GC Isolink, ThermoFisher). The GC column is as described above, while the oven temperature was programmed to 70 °C for 2 min followed by a 4 °C/min increment to 300 °C and held for 15 min. For calibration, a CO_2 standard gas was injected before and after each analysis. Each sample was analyzed twice. The mean isotope composition is reported in the δ notation in permil (‰) relative to the V-PDB standard. The average values of duplicate runs and analytical reproducibility per sample is less than 0.3‰.

4. Results

4.1. Carboniferous coal measures

In this section, bulk geochemical data for Carboniferous shale and coal samples are presented (Table 1). Detailed petrographic and geochemical data exist only for coal samples.

4.1.1. Bulk geochemical data of Carboniferous samples

TOC contents of coal samples range from 51.5 to 77.0 wt% and reflect different mineral contents. Hence, shaly coal (28.8 and 33.5 wt %), coaly shale (12.7–17.1 wt%) and shale samples (2.0–7.3 wt%) have lower TOC contents. In the main seam (#6), the TOC contents decrease towards the top (Fig. 3b) reflecting ash yields, which increase from the relative clean lower part of the seam (10 wt% ash yield dry basis [db]) to 46 wt%db (ash data are from Wolf et al., 1988).

Sulphur contents of coal samples are generally low. In the main seam, sulphur content (0.39 wt% in average) correlates well with TOC content (Fig. 3c). Somewhat higher sulphur contents (0.55–0.85 wt%) occur in seams below and above the main seam. Sulphur contents of shale samples are also very low (0.01–0.47 wt%). Consequently, TOC/S ratios for coal (81.2–193.1) and shale samples are very high (5.3–133.1).

HI values of shaly coal and coal samples vary between 143 and 261 mg HC/g TOC. The average HI in the main seam (#6) is 220 mgHC/gTOC (Fig. 3d). Between 1600 and 1740 m, a slight decrease in HI from ~240 to ~200 mgHC/gTOC is observed. HI values of coaly shale samples (149 and 181 mgHC/gTOC) are of similar order of magnitude, and those of shale samples (<10 wt%TOC) are generally lower (25–124 mgHC/gTOC; see also Fig. 4a). A plot of S_2 against TOC displays a good correlation (correlation coefficient for shale samples: $r^2 = 0.91$). The slope of the regression line gives a graphic solution of an average "true HI" (sensu Langford and Blanc-Valleron, 1990) of 131 mg HC/gTOC (Fig. 4b).

T_{max} values of coal (440–461 °C, average 450 °C) and shale samples (443–480 °C, avg. 456 °C) are similar and do not show a distinct depth trend in the interval between 1485 and 1835 m.

Shales samples are largely carbonate-free. Carbonate contents in coal samples reflect the presence of calcitic veins. The maximum carbonate content (11.2 wt%) is recorded in a sample from the main seam (#6; Fig. 3a).

4.1.2. Organic petrography

Maceral percentages of six samples from the main seam (#6) are

Table 1
Bulk geochemical parameters for Carboniferous sediments. Samples from the main seam (#6) are highlighted by grey shading.

Sample	Lithology/	Calcite	TOC	Sulphur	TOC/S	S_1	S_2	HI	T_{max}	PI	PP
ID[m]	Seam (#)	[Wt%]	[Wt%]	[Wt%]	[–]	[mg HC/g rock]		[mg HC/g TOC]	[°C]	[–]	[mg HC/g TOC]
1486.40	Coal	8.25	62.93	0.60	105	6.26	89.97	143	459	0.07	96
1494.74	Coal	3.07	69.33	0.85	81	5.75	135.12	195	450	0.04	141
1494.82	Shale	0.57	4.98	0.05	110	0.24	3.72	75	449	0.06	3.96
1556.00	Shale	0.46	3.79	0.03	108	0.24	2.04	54	466	0.11	2.28
1557.10	Shale	0.13	2.78	0.04	62	0.16	1.48	53	455	0.10	1.63
1557.40	Shale	0.08	3.79	0.06	61	0.24	2.81	74	450	0.08	3.05
1558.37	Shale	0.01	6.80	0.06	120	0.54	8.45	124	443	0.06	8.99
1558.50	Coal # 5	3.29	70.51	0.84	84	12.30	184	261	440	0.06	197
1559.40	Shale	0.74	7.29	0.05	133	0.61	6.50	89	457	0.09	7.11
1560.00	Coal # 5	6.75	72.19	0.55	130	10.15	168.32	233	448	0.06	178
1560.65	Shale	0.31	4.35	0.12	37	0.27	3.54	81	447	0.07	3.81
1561.95	Shale	0.00	5.82	0.07	86	0.48	5.74	99	452	0.08	6.22
1562.40	Coal #?	3.25	66.14	0.72	92	10.56	144.69	219	450	0.07	155
1566.50	Shale	0.20	2.01	0.38	5	0.09	0.50	25	459	0.15	0.58
1585.10	Coal # 6	0.00	57.06	0.43	133	8.39	126.56	222	447	0.06	135
1585.50	Shaly coal #6	11.23	33.52	0.23	147	5.57	68.75	205	448	0.07	74
1586.00	Coal # 6	0.00	51.47	0.41	126	7.38	116.89	227	451	0.06	124
1586.70	Coal # 6	0.12	54.81	0.31	178	7.34	116.43	212	449	0.06	124
1586.95	Coal # 6	0.00	74.78	0.44	170	9.83	154.60	207	451	0.06	164
1587.35	Coal # 6	0.00	69.53	0.40	175	9.35	145.63	209	448	0.06	155
1587.48	Coal # 6	1.68	65.27	0.41	159	10.01	147.23	226	453	0.06	157
1587.70	Coal # 6	0.00	74.51	0.44	169	10.48	171.90	231	447	0.06	182
1588.10	Coal # 6	3.64	53.38	0.30	176	7.11	118.34	222	448	0.06	125
1588.40	Coal # 6	0.00	69.54	0.50	139	9.56	164.43	236	448	0.05	174
1588.63	Coal # 6	1.26	66.10	0.40	163	9.52	162.03	245	448	0.06	172
1590.95	Coal # 6	0.00	75.69	0.44	170	9.64	166.55	220	451	0.05	176
1591.19	Coal # 6	0.00	76.95	0.40	193	10.14	156.86	204	448	0.06	167
1591.25	Shale	0.14	1.98	0.03	64	0.14	1.15	58	457	0.11	1.29
1617.60	Coaly Shale	0.87	17.05	0.25	69	1.54	30.83	181	448	0.05	32.36
1620.99	Shaly coal	1.32	28.84	0.24	119	3.06	52.49	182	451	0.06	56
1621.50	Shale	0.67	5.31	0.05	106	0.42	3.98	75	460	0.10	4.40
1623.00	Shale	0.37	3.17	0.05	67	0.22	1.66	52	465	0.11	1.88
1623.80	Shale	0.26	8.05	0.41	19	0.61	7.89	98	449	0.07	8.50
1654.04	Shale	0.21	6.31	0.05	126	0.55	5.33	84	462	0.09	5.87
1656.45	Shale	0.00	7.04	0.09	80	0.51	5.94	84	451	0.08	6.45
1656.67	Shale	0.04	3.69	0.05	76	0.19	1.67	45	457	0.10	1.86
1701.30	Coal # 9	4.36	75.52	0.62	122	11.75	157.21	208	459	0.07	169
1702.00	Shale # 9	0.48	5.70	0.05	118	0.55	5.57	98	451	0.09	6.11
1703.00	Coaly shale	0.12	12.72	0.15	83	1.53	19.00	149	457	0.07	20.52
1738.46	Coal # 10	0.76	68.55	0.58	118	9.40	132.37	193	455	0.07	142
1739.90	Coal # 10	0.00	65.31	0.66	100	8.28	132.08	202	461	0.06	140
1742.30	Shale	0.14	3.51	0.04	88	0.21	1.29	37	488	0.14	1.50
1834.15	Shale	0.04	5.10	0.06	85	0.37	4.82	95	456	0.07	5.19

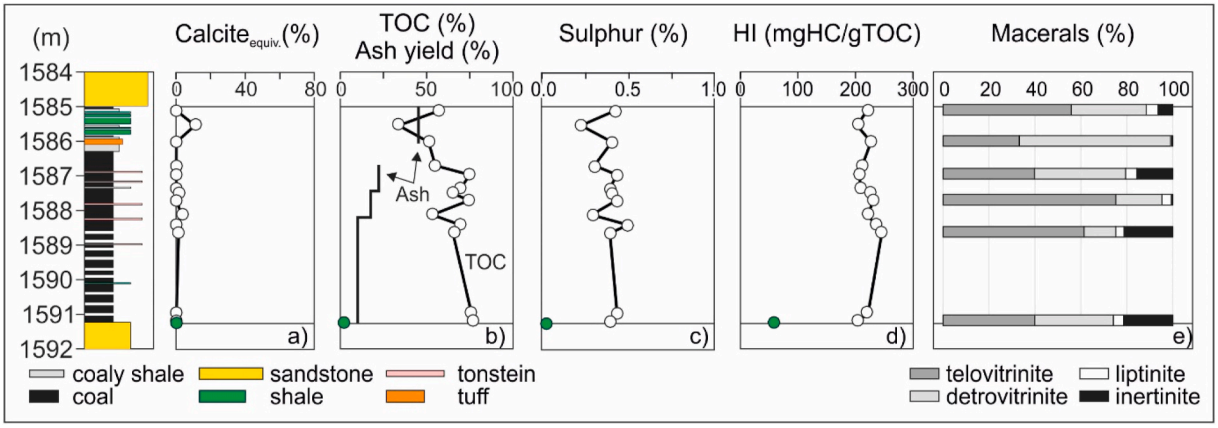

Fig. 3. Sketch of the main coal seam (#6) with vertical variation of bulk geochemical parameters and maceral percentages. Lithology and ash yield are from Wolf et al. (1988). Data from a shale sample from the underlying fine-grained sandstone are shown by green symbols.

presented in Table 2 and Fig. 3. The prevailing maceral group is vitrinite (74–99 vol%; 85 vol% in average). Telovitrinite (mainly collotelinite; Fig. 5) is more abundant than detrovitrinite (except in the sample from 1586.00 m depth). Inertinite macerals occur in significant amounts (up to 22 vol%; 11 vol% in average). Pyrofusinite (fossil charcoal; 6 vol% average; Fig. 5) dominates amongst the macerals of the inertinite group. Degradofusinite (fusinite formed due to degradation; 3 vol%), highly degraded macrinite (1.4 vol%), and intertodetrinite (0.7 vol%) are less

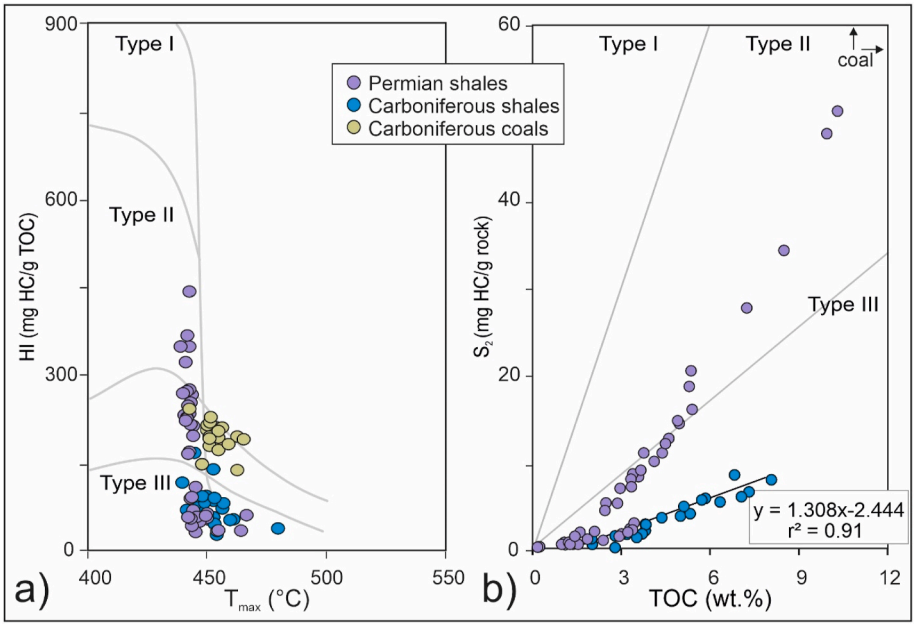

Fig. 4. Cross-plots of a) HI versus T_{max} and b) S_2 versus TOC. Data from coaly shales and coals (TOC >12 wt%) are not displayed in Fig. 4b. A regression line is plotted for Carboniferous shale samples. (Regression lines for different subsets of Permian shales are shown in Fig. 17).

Table 2
Maceral percentages and vitrinite reflectance in Carboniferous coals from the main seam #6. Std – standard deviation, n – number of measurements.

Sample ID	Telo-vitrinite	Detro-vitrinite	Degrado-fusinite	Pyro-fusinite	Inerto-detrinite	Macri-nite	Secreti-nite	Spori-nite	Cuti-nite	Resi-nite	Exsuda-tinite	Lipto-detrinite	Vitrinite Reflect.	Std. dev	n
[m]	[vol%]	[vol%]	[vol%]	[vol%]	[vol%]	[vol %]	[vol%]	[vol %]	[vol %]	[vol %]	[vol%]	[vol%]	[%Rr]		
1585.10	55.9	32.6	0.2	5.0	0.8	0.4	0.0	3.4	0.2	1.0	0.0	0.6	0.95	0.04	100
1586.00	33.2	65.9	0.0	0.2	0.4	0.0	0.0	0.2	0.2	0.0	0.0	0.0			
1586.95	39.8	39.7	4.9	8.0	0.5	2.3	0.0	4.0	0.0	0.0	0.7	0.2			
1587.70	75.2	20.2	0.2	0.0	0.0	0.4	0.0	3.8	0.0	0.0	0.0	0.2			
1588.63	61.4	13.8	10.6	6.8	0.4	2.2	1.2	3.2	0.4	0.0	0.0	0.0	0.91	0.04	100
1591.19	39.9	34.3	2.2	14.0	2.2	3.1	0.0	4.0	0.0	0.0	0.2	0.2			

abundant. Significant amounts of secretinite (oxidized plant excretions [ICCP, 1998]; Fig. 5) are limited to sample 1588.63 m (1.2 vol%). Liptinite contents range from 0.4 to 5.2 vol% (3.7 vol% in average). Sporinite (3.1 vol% in average) is the dominant liptinite macerals. Sporangia and macrosporinite are present (Fig. 5). Liptodetrinite, cutinite, resinite, and exsudatinite (solid residue of originally petroleum-like substances; Pickel et al., 2017) are rare. Vitrinite reflectance of two samples from the main seam is 0.91 and 0.95 %Rr (Table 2).

4.1.3. Biomarker

Representative GC-traces of three coal and one shale sample from the main coal seam #6 are shown in Fig. 6. Biomarker results of six coal and the shale sample from the main coal seam #6 are shown in Table 3. Depth plots of selected parameters are provided in Fig. 7. The extractable organic matter (EOM) content ranges from 18.2 to 29.0 mg/gTOC and is dominated by asphaltenes (avg. 66 wt%), followed by NSO compounds (avg. 24%), aromatic (avg. 6 wt%) and aliphatic (avg. 4 wt %) hydrocarbons, respectively.

The samples contain moderate concentrations of *n*-alkanes (73–612 μg/g TOC) ranging in chain length from *n*-C_{15} to *n*-C_{35} (Fig. 6). With the exception of the lowermost sample (1591.19 m), the unimodal distribution patterns show a peak at C_{24} or C_{25}. Mid-chain *n*-alkanes (*n*-C_{21-25}/∑*n*-alkanes: 0.40–0.42) are typically more abundant than long-chain (*n*-C_{27-31}/∑*n*-alkanes: 0.31–0.37) and short-chain *n*-alkanes (*n*-C_{15-19}/∑*n*-alkanes: 0.06–0.16; Table 3; Fig. 7a). The lowermost sample shows a peak at *n*-C_{17} and contains a relatively high amount of short-chain *n*-alkanes (0.30), but relatively low amounts of mid- (0.36) and long-chain *n*-alkanes (0.16). No marked odd-even predominance could be seen and the carbon preference index (CPI after Bray and Evans, 1961) ranges from 1.02 to 1.16 (Table 3).

The concentrations of isoprenoids are low (6–25 μg/g TOC). The pristane/phytane (Pr/Ph) ratios (Didyk et al., 1978) are very high, but slightly lower in the upper three samples (3.6–4.2) than in the lower three samples (4.5–4.9; Fig. 7b). The samples are characterized by moderate pristane/*n*-C_{17} ratios (0.90–2.00) and very low phytane/*n*-C_{18} ratios (0.20–0.43; Table 3).

In all samples, sterane concentrations are very low (4–9 μg/g TOC) and C_{29} steranes significantly dominate over C_{28} and C_{27} steranes ($C_{29} \gg C_{28} > C_{27}$; Fig. 7c). The C_{29} ααα sterane 20S/(20S + 20R) ratio ranges from 0.43 to 0.49 (avg. 0.45), while ratios of αββ/(αββ+ααα) C_{29}-steranes range from 0.43 to 0.60 (Table 3).

Hopanes are significantly more abundant (28–76 μg/g TOC) than steranes. Regular αβ hopanes from C_{27} to C_{35} dominated the distribution with C_{30} being most abundant, while C_{28} was absent. The Ts/(Ts + Tm) and moretane/hopane ratios are both ~0.1. The C_{35} homohopane index (HHI = C_{35}/C_{31-35}) is very low. The 22S/(22S + 22R) isomerization ratios of C_{31} hopanes (0.6) reached the equilibrium value (Peters et al., 2005). Tricyclic terpanes (TT) are present in low amounts (3–13 μg/g TOC). Prominent among them are the C_{19}, C_{20}, and C_{23} TTs (Fig. 6). C_{24} Tetracyclic terpane (TeT) is also present in significant amounts. The ratios of C_{19}/C_{23} TT (2.66–8.66) and C_{20}/C_{23} TT (2.71–7.12) are indicators for land-plants input (Noble et al., 1986; Peters et al., 2005) and

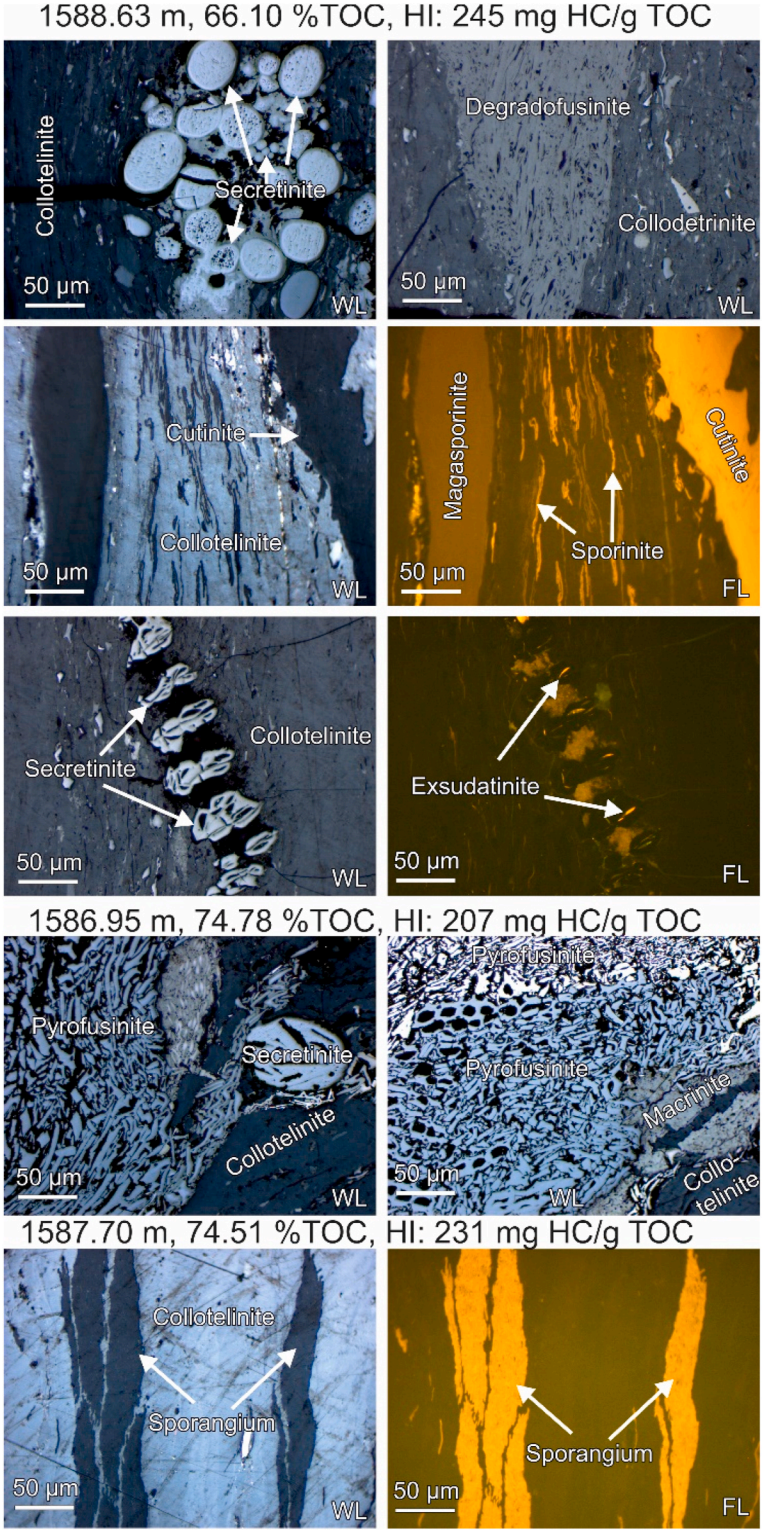

Fig. 5. Microphotographs of typical macerals in Carboniferous coal samples. (WL: white light, FL: fluorescent light).

are very high in all samples with exception of the uppermost coal sample (1581.10 m) and the shale sample from the floor of the seam (1591.25 m) where they are approximately 0.5 (Fig. 7d). Consequently, these ratios show an upward increasing-decreasing trend.

The dominant aromatic hydrocarbon compounds (Table 3) are naphthalene and its methylated counterparts (di, tri and tetra methyl-naphthalenes) followed by phenanthrene and its methylated counterparts (methyl-phenanthrenes (MP) and dimethyl-phenanthrenes (DMP)). The methyl-phenanthrene index (MPI-1 according to Radke et al., 1986; Radke, 1988) varies from 0.49 to 0.56 for the coals. Equivalent vitrinite reflectance values calculated from MPI-1 (Radke and Welte, 1983) range from 0.69 to 0.74 %Rr. The concentration of methyl-dibenzothiophene (MDBT; 0.77–1.55 µg/g TOC) and the dibenzothiophene/phenathrene (DBT/P; 0.01–0.02) ratio are very low.

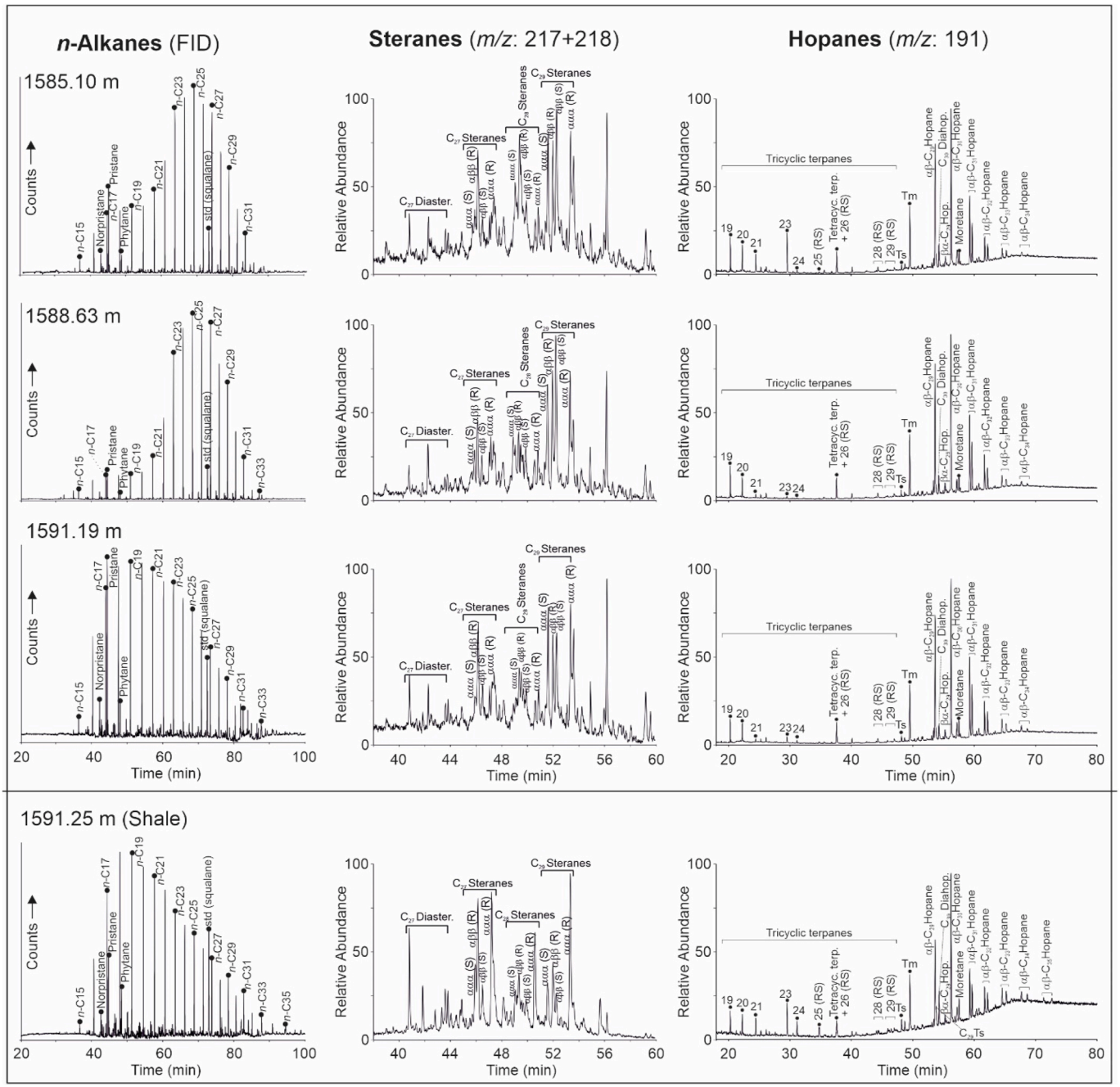

Fig. 6. Representative gas chromatograms of samples from the main coal seam (#6).

4.1.4. Compound-specific stable carbon isotopy

Carbon isotope compositions of *n*-alkanes with 22–29 carbon atoms and of pristane and phytane were determined (Table 4). The $\delta^{13}C$ values of *n*-alkanes and isoprenoids ranges from −26.33‰ to −28.58‰. In most samples, $\delta^{13}C$ values of *n*-alkanes decrease slightly (get isotopically lighter) with increasing carbon numbers. Only in the sample from 1586.00 m depth, $\delta^{13}C$ values remain constant or get slightly heavier (Fig. 8).

4.2. Permian Lacustrine Series

Forty-five shale samples and one driftwood sample (1314.23 m) from the Permian Lacustrine Series, covering the depth range from 1391.00 to 1194.08 m, were investigated. The shales are light grey, dark grey or dark brown and often contain fish scales and plant remains. Sampling gaps are due to the presence of sandy layers. The main focus is on the thickest shale interval in the lacustrine series (main shale interval; 1339.20–1326.95 m).

4.2.1. Bulk geochemical data of samples from the Permian Lacustrine Series

Largely carbonate-free shale samples with very low TOC contents (≤0.21 wt%), sulphur contents (≤0.10 wt%) and HI values (~20 mgHC/gTOC) occur near the base (1391.00 m) and in the upper part of the lacustrine series (1149.58–1194.08 m; Table 5).

Significantly higher TOC contents (0.95–10.25 wt%, 4.7 wt% in average) are observed in shale samples in the depth interval between 1358.90 and 1310.08 m (Table 5; Fig. 9). HI values in this interval range from 24 to 488 mgHC/gTOC and indicate the presence of Type II, III and IV kerogen (Fig. 4a). The plot of S_2 versus TOC also reflects the presence of different kerogen types (Fig. 4b). As expected in fresh water lacustrine

Table 3
Concentration and concentration ratios of compound groups within the hydrocarbon fractions of Permian and Carboniferous sediments from the Weiach-1 well. Carboniferous coal samples in grey highlight. n.d = not detected.

Sample ID [m]	EOM [mg/gTOC]	Aliphatic [wt.%]	Aromatic [wt.%]	NSO compounds [wt.%]	Asphaltene [wt.%]	n-C15-19/ n-alkanes	n-C21-25/ n-alkanes	n-C27-31/ n-alkanes	CPI	Pr/Ph	Pr/C17	Pr/C18	Steranes [µg/g TOC]	C27/ C27-29 steranes	C28/ C27-29 steranes	C29/ C27-29 steranes
1310.08	15.31	8.28	10.11	60.46	21.15	0.35	0.29	0.19	1.17	1.17	0.73	0.58	54	0.34	0.29	0.37
1310.58	18.25	16.71	22.28	50.93	10.08	0.37	0.33	0.12	0.97	1.72	0.93	0.48	238	0.38	0.28	0.34
1311.55	24.47	12.05	16.33	62.25	9.37	0.45	0.29	0.12	1.13	3.01	2.66	1.00	146	0.36	0.26	0.38
1312.95	48.88	31.88	17.69	48.37	2.06	0.44	0.26	0.09	1.05	2.53	0.75	0.31	117	0.32	0.24	0.45
1313.37	61.42	38.44	13.26	45.71	2.59	0.40	0.29	0.11	1.17	2.55	0.66	0.26	99	0.39	0.32	0.29
1326.95	16.31	14.53	18.44	44.69	22.35	0.36	0.33	0.12	1.07	1.05	0.67	0.42	242	0.35	0.30	0.35
1328.65	29.33	12.46	6.09	53.62	27.83	0.33	0.39	0.10	1.17	0.85	0.08	0.06	29	0.45	0.19	0.37
1329.35	69.20	27.65	11.22	46.79	14.34	0.54	0.25	0.04	1.15	1.89	0.13	0.07	1	0.51	0.11	0.38
1330.15	39.20	21.72	7.81	53.15	17.32	0.58	0.24	0.03	1.10	2.11	0.08	0.03	14	0.47	0.13	0.40
1331.10	41.97	21.33	6.58	55.75	16.34	0.59	0.23	0.02	1.11	2.21	0.08	0.03	12	0.50	0.13	0.37
1332.43	48.11	23.33	7.39	50.39	18.88	0.58	0.24	0.02	1.26	0.99	0.07	0.06	17	0.52	0.13	0.35
1333.30	53.24	27.70	7.12	48.18	17.00	0.56	0.24	0.03	1.11	1.95	0.07	0.03	15	0.54	0.12	0.34
1334.22	51.80	25.16	8.01	50.38	16.46	0.55	0.26	0.04	1.11	1.54	0.13	0.07	24	0.48	0.16	0.36
1335.75	41.95	11.46	7.80	45.49	35.24	0.55	0.26	0.04	1.31	1.36	0.07	0.04	8	0.49	0.19	0.32
1336.12	57.53	24.45	5.94	56.73	12.88	0.53	0.26	0.05	1.14	1.98	0.14	0.06	27	0.46	0.15	0.40
1337.40	68.67	24.81	7.77	57.22	10.20	0.53	0.26	0.05	1.15	1.81	0.17	0.09	27	0.46	0.15	0.39
1338.35	63.96	23.78	12.21	53.75	10.26	0.53	0.26	0.06	1.15	2.49	0.19	0.08	27	0.39	0.15	0.45
1339.20	60.35	20.51	8.87	52.13	18.50	0.45	0.30	0.09	1.25	2.45	0.27	0.10	2	0.44	0.21	0.35
1350.70	25.98	20.29	14.54	59.74	5.43	0.43	0.31	0.10	1.20	1.74	0.33	0.20	23	0.38	0.26	0.36
1350.95	27.85	26.29	13.73	55.15	4.83	0.36	0.34	0.13	1.20	2.13	0.49	0.22	56	0.33	0.30	0.37
1358.90	11.75	9.03	10.11	63.54	17.33	0.41	0.30	0.13	1.37	1.06	0.46	0.38	9	0.43	0.26	0.31
1585.10	23.82	2.97	5.80	24.60	66.63	0.13	0.40	0.31	1.14	4.17	2.00	0.43	9	0.15	0.40	0.44
1586.00	21.95	4.72	7.81	25.17	62.30	0.11	0.40	0.32	1.16	3.88	1.36	0.29	7	0.14	0.31	0.55
1586.95	27.12	1.44	4.12	14.99	79.44	0.16	0.42	0.26	1.11	3.63	0.90	0.20	4	0.14	0.28	0.58
1587.70	28.96	5.13	6.40	19.77	68.70	0.08	0.41	0.36	1.14	4.60	1.31	0.27	8	0.17	0.29	0.54
1588.63	26.27	7.92	8.31	30.95	52.81	0.06	0.41	0.37	1.14	4.93	1.77	0.34	8	0.17	0.26	0.57
1591.19	22.01	2.06	6.53	26.20	65.21	0.30	0.36	0.16	1.02	4.51	1.65	0.30	7	0.22	0.21	0.56
1591.25	18.16	3.31	10.22	62.71	23.76	0.30	0.34	0.16	1.08	1.65	0.85	0.43	35	0.38	0.28	0.33

Sample ID[m]	S/(S + R) C29 Steranes	αββ/(αββ+ααα) C29 Steranes	C27 (Diast./Reg. Sterane)	Hopane [µg/g TOC]	Steranes/ Hopanes	S/(S + R) C31 Hopanes	Moretane/ Hopane	Ts/ (Ts + Tm)	Gam./ (Gam. + C30 Hopane)	C35/C31 - 35 Hopanes	Tricyclic terpanes Σ [µg/g TOC]	C19/ C23	C20/ C23
1310.08	0.25	0.37	0.21	96	0.56	0.59	0.36	0.07	0.06	0.05	12	0.46	0.83
1310.58	0.32	0.29	0.21	1697	0.14	0.58	0.45	0.03	0.06	0.02	77	0.61	1.10
1311.55	0.40	0.29	0.24	2305	0.06	0.59	0.41	0.02	0.10	0.01	160	0.99	1.63
1312.95	0.68	0.35	0.30	2963	0.04	0.58	0.19	0.67	0.17	0.08	281	0.78	1.04
1313.37	0.46	0.48	0.37	943	0.10	0.60	0.21	0.71	0.27	0.05	163	0.58	0.84
1326.95	0.25	0.29	0.16	262	0.92	0.59	0.25	0.27	0.12	0.09	42	0.19	0.36
1328.65	0.63	0.63	0.70	391	0.08	0.57	0.39	0.05	0.05	0.02	90	6.18	18.74
1329.35	0.64	0.36	1.25	8	0.07	0.55	0.19	0.76	0.31	n.d	2	0.54	0.32
1330.15	0.63	0.41	0.86	122	0.11	0.57	0.26	0.58	0.24	0.02	24	1.66	2.80
1331.10	0.57	0.42	0.82	102	0.11	0.57	0.26	0.63	0.24	0.02	21	1.84	1.34
1332.43	0.55	0.38	0.82	191	0.09	0.58	0.25	0.61	0.21	0.03	25	1.45	0.43
1333.30	0.71	0.28	0.79	153	0.10	0.57	0.23	0.68	0.28	0.03	25	1.15	0.31
1334.22	0.60	0.34	0.92	305	0.08	0.58	0.19	0.70	0.40	0.04	46	0.74	0.32
1335.75	0.68	0.47	0.87	64	0.12	0.57	0.27	0.34	0.23	0.03	12	0.92	0.35
1336.12	0.70	0.36	0.94	234	0.12	0.58	0.20	0.72	0.41	0.04	40	0.70	0.98
1337.40	0.58	0.34	0.88	272	0.10	0.58	0.20	0.70	0.31	0.03	54	0.72	0.37
1338.35	0.54	0.29	0.71	380	0.07	0.58	0.23	0.71	0.15	0.04	62	1.10	0.75
1339.20	0.70	0.54	1.10	10	0.16	0.58	0.27	0.50	0.14	0.04	3	1.38	2.26
1350.70	0.45	0.33	0.33	113	0.21	0.60	0.34	0.29	0.18	0.06	48	1.16	1.15
1350.95	0.27	0.32	0.25	86	0.65	0.61	0.33	0.46	0.23	0.07	35	0.58	0.86
1358.90	0.29	0.35	0.28	24	0.39	0.59	0.32	0.07	0.05	0.07	9	0.53	0.86
1585.10	0.44	0.49	0.45	72	0.13	0.61	0.10	0.07	n.d	0.01	13	0.52	0.52
1586.00	0.49	0.60	0.32	53	0.13	0.61	0.10	0.08	n.d	0.02	7	4.87	4.80
1586.95	0.44	0.56	0.41	28	0.15	0.61	0.12	0.09	n.d	0.01	3	5.21	4.22
1587.70	0.45	0.57	0.31	63	0.12	0.61	0.12	0.10	n.d	0.02	6	8.10	5.78
1588.63	0.43	0.53	0.26	63	0.13	0.61	0.12	0.09	n.d	0.02	6	8.66	7.12
1591.19	0.47	0.43	0.29	76	0.09	0.61	0.11	0.09	n.d	0.02	7	2.66	2.71
1591.25	0.22	0.33	0.26	38	0.92	0.60	0.15	0.18	0.11	0.09	8	0.47	0.53

Sample ID[m]	MP [µg/g TOC]	DMP [µg/g TOC]	MPI-1	Rc	MDBT [µg/g TOC]	DBT/ Phen	Aryl-isoprenoid [µg/g TOC]	AIR C13-17/C18-22	C30 (Diahop./Hop.)	Σ Tricyclic terpane/ Σ Hopane	Retene [µg/g TOC]	Simonellite [µg/g TOC]
1310.08	33	39	0.37	0.62	1	0.00	2	0.21	0.05	0.13	n.d	n.d
1310.58	21	3	0.22	0.53	n.d	0.00	3	0.08	0.04	0.05	n.d	n.d
1311.55	14	7	0.19	0.51	2	0.02	15	0.44	0.05	0.07	n.d	n.d

(*continued on next page*)

Table 3 (*continued*)

Sample ID[m]	MP [µg/g TOC]	DMP [µg/g TOC]	MPI-1	Rc	MDBT [µg/g TOC]	DBT/ Phen	Aryl-isoprenoid [µg/g TOC]	AIR C13-17/C18-22	C30 (Diahop./Hop.)	Σ Tricyclic terpane/ Σ Hopane	Retene [µg/g TOC]	Simonellite [µg/g TOC]
1312.95	11	41	0.24	0.54	12	0.12	58	2.55	0.31	0.09	n.d	n.d
1313.37	21	75	0.48	0.69	14	0.16	81	2.18	0.48	0.17	n.d	n.d
1326.95	24	17	0.35	0.61	1	0.01	6	0.08	0.11	0.16	n.d	n.d
1328.65	21	41	0.61	0.77	3	0.02	2	0.17	0.05	0.23	17.47	74.84
1329.35	32	70	0.53	0.72	7	0.02	24	1.01	0.40	0.23	5.78	21.29
1330.15	28	61	0.52	0.71	4	0.02	6	0.61	0.35	0.20	6.23	42.61
1331.10	25	48	0.53	0.72	3	0.02	7	0.65	0.41	0.20	5.87	17.69
1332.43	32	68	0.52	0.71	3	0.02	7	0.38	0.36	0.13	1.53	1.10
1333.30	33	82	0.52	0.71	3	0.02	9	0.55	0.44	0.16	1.41	0.76
1334.22	34	76	0.51	0.71	4	0.04	9	0.62	0.39	0.15	1.91	1.61
1335.75	26	62	0.55	0.73	4	0.02	3	0.21	0.22	0.19	1.78	0.75
1336.12	26	65	0.54	0.72	3	0.02	7	0.47	0.42	0.17	1.26	0.33
1337.40	22	59	0.53	0.72	3	0.03	11	0.59	0.48	0.20	1.33	1.09
1338.35	25	71	0.56	0.74	6	0.03	21	0.97	0.56	0.16	4.30	10.61
1339.20	38	110	0.57	0.74	8	0.03	21	0.58	0.36	0.34	6.12	22.26
1350.70	28	13	0.16	0.50	2	0.00	12	0.42	0.29	0.42	n.d	n.d
1350.95	17	18	0.17	0.50	n.d	0.01	14	0.18	0.35	0.40	n.d	n.d
1358.90	38	29	0.48	0.69	1	0.01	1	0.33	0.07	0.39	n.d	n.d
1585.10	47	58	0.54	0.73	1	0.01	n.d	n.d	0.17	0.18	n.d	n.d
1586.00	66	84	0.53	0.72	2	0.01	n.d	n.d	0.10	0.12	n.d	n.d
1586.95	52	55	0.53	0.72	1	0.02	n.d	n.d	0.12	0.11	n.d	n.d
1587.70	45	53	0.56	0.74	1	0.02	n.d	n.d	0.13	0.10	n.d	n.d
1588.63	48	71	0.52	0.71	1	0.02	n.d	n.d	0.13	0.09	n.d	n.d
1591.19	52	74	0.49	0.69	1	0.02	n.d	n.d	0.12	0.09	n.d	n.d
1591.25	76	71	0.53	0.72	2	0.02	3	0.08	0.23	0.21	n.d	n.d

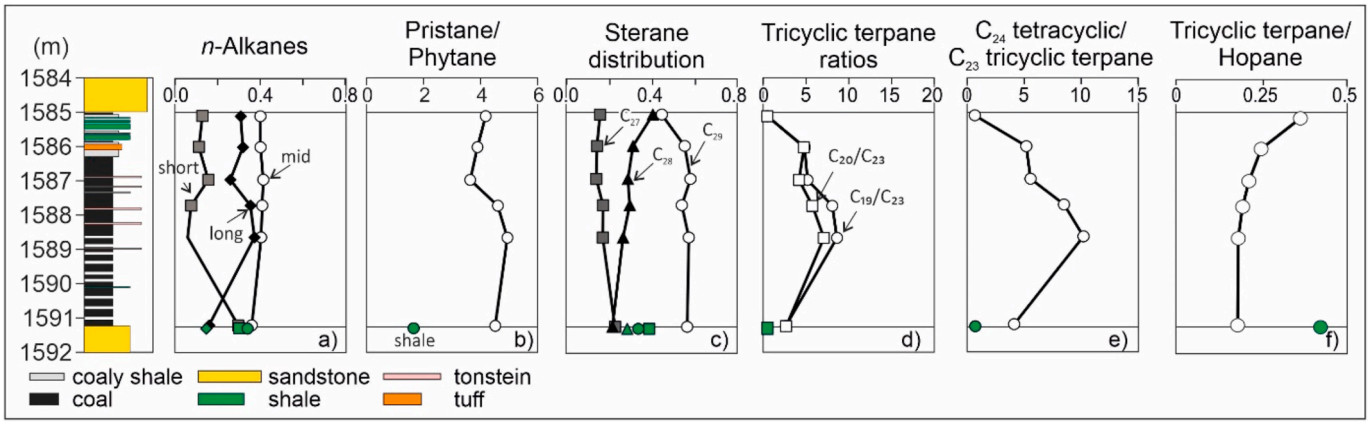

Fig. 7. Depth plots of selected geochemical parameters in the main seam (#6). Data from the underlying shale are shown by green symbols.

sediments, sulphur contents are generally low (<0.8 wt%), despite high TOC contents. This results in high TOC/S ratios (5.8–197). Carbonate contents are often very low (<1.0 wt%), but significantly higher values occur between 1351.0 and 1350.3 m (max. 31 wt%), at the base (1339.2–1338.3 m; max. 37 wt%), near the top of the main shale interval (1328.7–1327.6 m; max. 8 wt%), and in the shale interval between 1310.5 and 1314.3 m (max: 23 wt%). Both, TOC and HI decrease upwards in the main shale interval (1326.9–1339.2 m), although a TOC and HI peak occurs at 1329.35 m depth, briefly interrupting this trend (Fig. 9).

The investigated driftwood (1314.23 m) has a very high TOC content (51.20 wt%) and a low HI (155 mgHC/gTOC). The sulphur content of the driftwood is relatively high (1.46 wt%).

The average T_{max} values of Permian samples with $S_2 > 0.2$ mgHC/g rock is 442 °C (435–460 °C). No depth trend is visible in the depth interval between 1310 and 1391 m.

4.2.2. *Organic Petrography and palynofacies*

Organic petrographic and palynofacies investigations have been performed on twelve samples from the main shale interval (1339.20–1328.65 m).

The prevailing maceral group within the main shale interval is liptinite (18–79 vol%) closely followed by inertinite (8–63 vol%) and vitrinite (5–43 vol%; Table 6; Fig. 10). Main liptinite macerals include alginite and liptodetrinite (Fig. 10a,b,c). Telalginite is typically more abundant than lamalginite and includes some *Botryococcus*-type algal bodies (Fig. 10c). Sporinite (Fig. 10d) is typically rare. The mineral matrix is strongly fluorescing (e.g. Fig. 10a) suggesting that not all organic matter is visible microscopically. Five samples were selected for vitrinite reflectance measurements (Table 6). Strongly varying reflectance values with high standard deviations show that the reflectance of vitrinite particles varies considerably within and between the samples. Thus, vitrinite reflectance in the short interval varies from 0.56 (±0.19) to 0.78 (±0.11) %Rr. The mean value is 0.66 %Rr. This value is consistent with previously published data (NAGRA, 2002) and is lower than that of the deeper coal seams.

Amorphous organic matter (AOM; Fig. 11) is the main component in palynofacies in both non-filtered and filtered slides. It represents 55 to 98 vol% (avg. 70 vol%) of the particles in the filtered slides (Table 6; Fig. 12), but may be invisible in reflected light mcroscopy. Two types of

Table 4
Compound specific carbon isotope ratios ($\delta^{13}C$; ‰) of Permo-Carboniferous samples of Weiach-1. Coal samples in grey highlight.

Sample ID [m]	*n*-C_{15}	*n*-C_{16}	*n*-C_{17}	*n*-C_{18}	*n*-C_{19}	*n*-C_{20}	*n*-C_{21}	*n*-C_{22}	*n*-C_{23}	*n*-C_{24}	*n*-C_{25}	*n*-C_{26}	*n*-C_{27}	*n*-C_{28}	*n*-C_{29}	Pristane	Phytane
1312.95	*n.d*	−27.63	−28.07	−28.43	−28.90	−29.59	−29.86	−30.13	−30.43	−29.80	−30.99	*n.d*	*n.d*	*n.d*	*n.d*	−25.90	−26.36
1313.37	*n.d*	−28.15	−28.52	−28.94	−29.63	−29.69	−30.21	−30.52	−30.69	−30.60	−31.24	−30.15	−30.32	*n.d*	*n.d*	−26.74	−27.63
1328.65	*n.d*	*n.d*	*n.d*	−30.31	−30.31	−30.90	−30.22	−30.72	−30.67	−30.68	−31.08	−31.07	−30.65	−30.32	*n.d*	*n.d*	*n.d*
1329.35	−28.58	−28.99	−29.23	−29.79	−29.93	−30.00	−30.21	−30.25	−29.93	−29.49	−29.81	−29.51	−28.97	−29.12	−28.87	−28.47	−28.87
1330.15	*n.d*	−28.44	−29.09	−29.89	−29.74	−29.95	−29.89	−29.74	−29.24	−29.03	−29.00	−28.90	−28.27	−28.77	−28.89	−28.65	−28.80
1331.10	*n.d*	−28.68	−28.94	−29.52	−29.75	−29.85	−29.69	−29.64	−29.38	−29.18	−29.04	−28.22	−27.96	−28.32	−28.18	−29.10	−29.22
1332.43	*n.d*	−29.15	−29.38	−29.11	−28.93	−28.91	−28.77	−28.74	−29.19	−29.26	−29.37	−28.67	−27.86	−28.16	−28.32	−28.92	−28.79
1333.30	*n.d*	−29.45	−29.44	−29.19	−29.06	−29.18	−29.11	−29.42	−29.25	−29.17	−29.18	−29.39	−29.35	−29.01	−29.21	−28.83	−29.00
1334.22	−29.95	−29.21	−29.64	−29.63	−29.49	−29.63	−29.30	−29.31	−29.17	−28.70	−28.79	−29.24	−28.85	−28.51	−28.72	−29.58	−29.53
1335.75	*n.d*	−28.89	−29.17	−29.41	−29.44	−29.81	−30.00	−30.42	−30.18	−29.83	−30.28	−30.03	−29.65	−29.78	−30.05	−29.43	−29.79
1336.12	−29.43	−29.38	−29.86	−30.03	−30.07	−30.27	−30.43	−30.82	−31.20	−30.50	−30.27	−30.61	−31.03	−31.12	−30.73	−30.21	−30.21
1337.40	−29.54	−29.63	−30.04	−30.32	−30.29	−30.50	−30.62	−31.10	−30.64	−30.99	−30.40	−30.88	−30.88	−31.07	−30.87	−30.17	−29.93
1338.35	−28.90	−29.32	−29.78	−29.71	−29.59	−29.47	−29.87	−30.12	−30.91	−30.51	−30.37	−30.64	−31.14	−30.62	−30.45	−29.91	−30.28
1339.20	−29.08	−30.17	−29.96	−29.92	−29.97	−30.04	−30.61	−31.09	−31.22	−30.72	−30.67	−30.63	−31.03	−30.93	−31.15	−30.27	−30.33
1350.95	*n.d*	*n.d*	*n.d*	−28.10	−29.37	−29.64	−30.10	−29.72	−30.94	−31.15	−31.49	−28.94	−30.96	−30.39	*n.d*	*n.d*	−28.76
1585.10								−26.33	−26.82	−26.85	−27.03	−26.60	−27.00	−27.09	−27.82	*n.d*	*n.d*
1586.00								−27.65	−27.85	−27.47	−27.72	−27.83	−27.94	−27.45	−27.32	*n.d*	−27.06
1586.95								−26.84	−26.87	−25.97	−26.80	−26.31	−27.05	−27.31	*n.d*	*n.d*	*n.d*
1587.70								−26.94	−27.43	−27.76	−28.42	−28.58	−28.55	−28.53	*n.d*	−28.10	−26.48
1588.63								*n.d*	−27.12	−28.03	−28.08	−28.02	−28.20	−28.09	*n.d*	−27.93	−27.28

AOM particules were observed in the Weiach-1 samples. The first AOM type corresponds to large, grey particles with a sub-rectangular shape. Such sub-rectangular shape organic forms of AOM are known to possibly originate from degraded translucent phytoclast tissues such as cuticles or lignocellulosic tissues (Laggoun-Défarge et al., 1999; Sebag et al., 2006). The second AOM type is characterized by orange to grey-orange fluffy clouds. This AOM type is generally interpreted as deriving from algal/bacterial matter living in the upper part of the water column (Tyson, 1995). Transitional forms exist between these two AOM types. Therefore, in some slides it is not easy to distinguish between these two end members. The two AOM types co-occur in many samples (Fig. 12), but grey, sub-rectangular AOM tends to dominate in deeper samples (1339.20–1334.22 m), whereas orange cloudy AOM particles dominate from 1333.30 m to 1328.65 m (Table 6). However, sub-rectangular AOM again shortly dominates at 1329.35 m (Fig. 12), corresponding to a peak in TOC and HI values (see above). Palynomorphs (spores and pollen) represent 0.5 to 22 vol% (10.6 vol% in average) of the particles in palynofacies. Opaque phytoclasts represent 1.4%–23.30% (average 12.4 vol%) of palynofacies and are much more abundant than translucent phytoclasts (0.5–10.4 vol%; avg. 5.7 vol%) (Table 6). Some opaque phytoclasts show recognizable biological wood structures. Opaque and translucent phytoclast proportions increase regularly from 1338.35 to 1331.1 m/1330.15 m (Fig. 12). *Botryococcus* algae are observed in trace amounts (<1 vol%) within half of the studied slides. Hyphae from fungi also appear in trace amounts (<1 vol%) within most slides.

In general there is no good relationship between maceral percentages and HI. However, moderate positive and negative correlations between HI and AOM ($r^2 = 0.58$) and opaque phytoclasts ($r^2 = 0.60$) can be observed, respectively.

4.2.3. Biomarker

Rock extracts from 21 Permian shale samples (1310–1360 m) were investigated, twelve of which come from the main shale interval. The EOM ranges from 11.7 to 69.2 mg/gTOC (41.7 mg/gTOC on average) and is dominated by NSO compounds (53 wt% in average). Aliphatic hydrocarbons (21 wt% in average), asphaltenes (15 wt% in average) and aromatic hydrocarbons (11 wt% in average) occur in lower amounts. A positive correlation exists between EOM and HI ($r^2 = 0.65$). Representative GC-FID and GC-MS traces are shown in Fig. 13. Concentrations and ratios of selected molecular compounds are listed in Table 3 and plotted versus depth in Fig. 14.

4.2.3.1. n-Alkanes and isoprenoids. The concentrations of *n*-alkanes (>*n*-C_{15} fraction) vary significantly between 82 and 7392 μg/gTOC. Typically, their chain lengths range from *n*-C_{15} to *n*-C_{35} and show a unimodal chain length distribution (Fig. 13). Short-chain *n*-alkanes (*n*-$C_{15–19}/\sum n$-alkanes: 0.33–0.59) are more abundant than mid-chain (*n*-$C_{21–25}/\sum n$-alkanes: 0.23–0.39), while low long-chain *n*-alkanes are rare (*n*-$C_{27–31}/\sum n$-alkanes: 0.02–0.19) (Table 3; Fig. 14a). The maximum amounts of long chain *n*-alkanes (>0.5) and the minimum amounts of long chain *n*-alkanes (<0.07) are observed in the middle part of the main shale interval. CPI values (Bray and Evans, 1961) vary from 0.97 to 1.37 and show a clear upward decrease (Fig. 14b).

Isoprenoid concentrations vary from 9 to 822 μg/gTOC. The Pr/Ph ratio ranges between 0.85 and 3.01. Similar to CPI, Pr/Ph ratios in the main shale interval decrease upwards (Fig. 14c). However, no clear trend is visible below and above this interval. The Pr/*n*-C_{17} (0.07–2.66) and the Ph/*n*-C_{18} (0.03–1.0) ratios (Fig. 14o) show similar depth trends as the relative amount of long chain *n*-alkanes.

4.2.3.2. Steroids distribution. Sterane concentrations are low within and below the main shale interval (1–56 μg/g TOC) and relatively high above it (54–242 μg/g TOC). Sterane distributions are generally dominated by C_{27} steranes. This is especially true for the central part of the

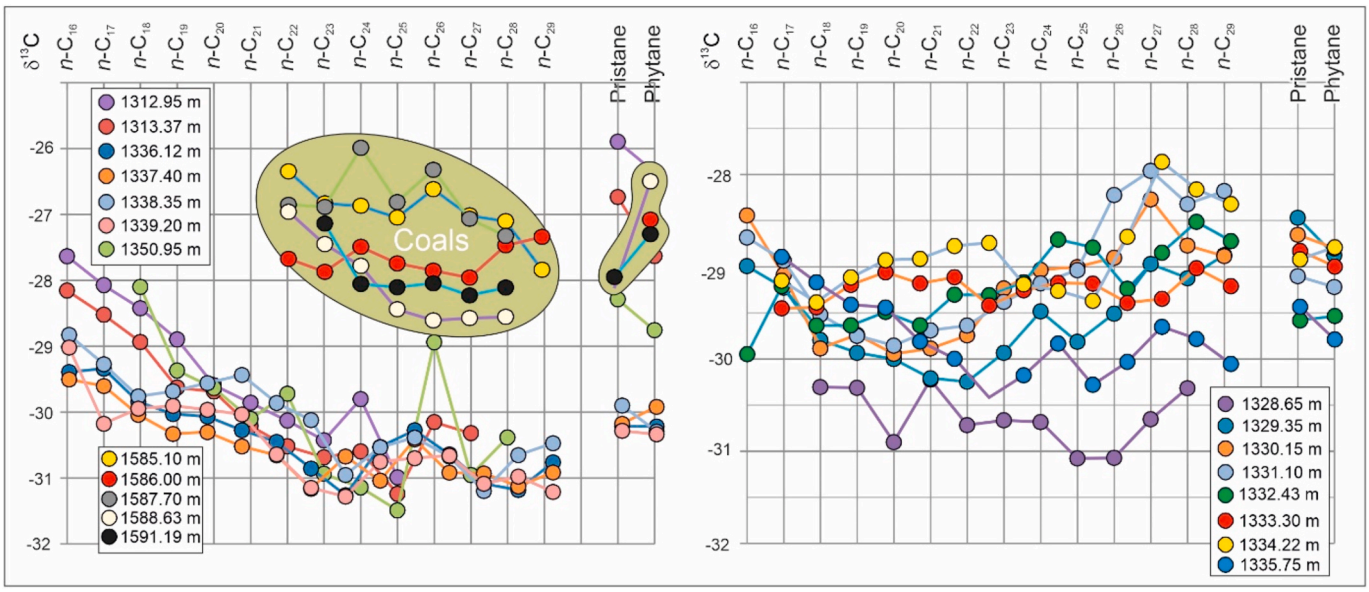

Fig. 8. Carbon isotope composition of individual *n*-alkanes, pristane and phytane for Permian shales and Carboniferous coal samples from different stratigraphic intervals in the Weiach-1 well.

main shale interval (1337.40–1328.65 m), where C_{29} and C_{28} steranes occur in significantly lesser amounts. Below and above of this interval, concentrations of C_{27} and C_{29} steranes are similar (Fig. 14d; Table 3). The C_{29} ααα sterane 20S/(20S + 20R) ratio ranges from 0.25 to 0.71, while ratios of αββ/(αββ+ααα) C_{29}-steranes range from 0.28 to 0.63 (Fig. 14p,q; Table 3). Low 20S/(20S + 20R) ratios are mainly found in samples with high proportions of long chain *n*-alkanes.

4.2.3.3. Penta- and tricyclic triterpanes. Similar to the Carboniferous coal samples, hopanes are significantly more abundant than steranes. Especially high hopane concentrations (943–2963 μg/g TOC) are found in four samples between 1310.58 and 1313.37 m depth. Elsewhere, hopane concentrations range from 8 to 391 μg/g TOC.

Their mass chromatograms (Fig. 13) show the presence of similar compounds as in the Carboniferous succession. The C_{35} homohopane index (HHI = $C_{35}/C_{31\text{-}35}$) decreases upwards in the lower part of the lacustrine series, including the main part of the main shale interval. However, the C_{34} to C_{35} peaks are extremely small in most cases. The C_{31} hopane 22S/(22S + 22R) isomerization ratios (0.55–0.61; Table 3) are close to the end-point value (Mackenzie and Maxwell, 1981). The Ts/(Ts + Tm) ratios vary between 0.02 and 0.76 with the lowest values occurring below and above the main shale interval (Fig. 14h). Moretane/hopane ratios (0.20–0.45) and Ts/(Ts + Tm) ratios (0.02–0.76) show a strong negative correlation ($r^2 = 0.82$). The latter also shows a moderate negative correlation with the relative percentage of long chain *n*-alkanes ($r^2 = 0.50$). The Gammacerane Index ranges from 0.05 to 0.41 and reaches maximum values in the main shale interval (Fig. 14i).

Concentrations of tricyclic terpanes (TT) are low (2–281 μg/g TOC; Table 3) and positively correlated with hopanes ($r^2 = 0.82$). Similar to hopanes, the highest concentrations occur above the main shale interval. In most samples, tricyclic terpanes occur within the C_{19} to C_{29} chain length with C_{19}, C_{20}, C_{23} being the most prominent and C_{27} being absent. Ratios for C_{19}/C_{23} TT and C_{20}/C_{23} TT were plotted against depth (Fig. 14j; Table 3).

4.2.3.4. Aromatic hydrocarbons. The Permian shales contain very low concentrations of benzenes, naphthalenes, phenanthrenes, dibenzothiophenes and their alkylated equivalents (Table 3). The methyl phenanthrene index (MPI-1) in the main shale interval varies from 0.51 to 0.61, while lower values (0.16–0.48) occur below and above this interval. Equivalent vitrinite reflectance values calculated from MPI-1 within the main shale interval range from 0.71 to 0.74% and are slightly lower (0.51–0.69) below and above this interval. Methyl dibenzothiophene (MDBT) concentrations are very low (1.16–14.34 μg/g TOC), the highest values occur in two samples above the main shale interval. The dibenzothiophene/phenathrene (DBT/P) ratios are generally low (<0.05), higher values are limited to the depth between 1313.37 and 1312.95 m (Fig. 14k). Low amounts of mono- (0.15–1.39 μg/g TOC) and tri-aromatic steroids (0.07–1.29 μg/g TOC) are present.

Aryl isoprenoids with C_{13} to C_{23} chain length are present and have low to moderate concentrations (1.06–81.14 μg/g TOC; Fig. 14m). Maximum concentrations occur in the depth interval (1313.37–1312.95 m) with high DBT/P ratios. The aryl isoprenoid ratio (AIR = $C_{13\text{-}17}/C_{18\text{-}22}$) (0.08–2.55; Table 3) shows a strong positive correlation with the total amount of aryl isoprenoids ($r^2 = 0.85$).

Polycyclic aromatic hydrocarbons (PAHs), such as simonellite and retene, were determined within the main shale interval with significant concentrations (0.33–74.84 μg/g TOC and 1.26–17.47 μg/g TOC, respectively). Both compounds exhibit similar depth trends (Fig. 14p).

4.2.4. Compound-specific stable carbon isotopy

Carbon isotope ratios of *n*-alkanes with 15–29 carbon atoms and for pristane and phytane were determined for twelve samples within the main shale interval, one sample below and two samples above (Table 4). In Fig. 8, $\delta^{13}C$ values of *n*-alkanes are plotted versus their chain length. Two different patterns can be recognized: Samples from the lower part of the shale interval (1350.95–1336.12 m), as well as of samples above (1313.37–1312.95 m) and below this interval (1350.95 m) are characterized by *n*-alkanes, which become isotopically lighter with increasing chain length. In addition, the $\delta^{13}C$ values of specific *n*-alkanes vary in a relatively narrow range. In contrast, $\delta^{13}C$ values of *n*-alkanes from samples from the upper part of the main shale interval (1335.75–1328.65 m) vary considerably and long chain n-alkanes typically have less negative $\delta^{13}C$ values than shorter chain *n*-alkanes.

Stratigraphic variations of $\delta^{13}C$ values of *n*-alkanes and isoprenoids are shown in Fig. 15. Different depth trends are observed for *n*-alkanes with different chain lengths, pristane and phytane.

- $\delta^{13}C$ values of pristane and phytane are about −28 to −29‰ at 1350.95 m depth and increase approximately from −30 to −25‰ in

Table 5
Bulk geochemical parameters of samples from the Permian Lacustrine Series. Samples from the main shale interval are highlighted by grey shading.

Sample	Lithology	Calcite	TOC	Sulphur	TOC/S	S_1	S_2	HI	T_{max}	PI	PP
ID [m]		[Wt.%]	[Wt.%]	[Wt.%]	[–]	[mg HC/g rock]		[mg HC/g TOC]	[°C]	[–]	[mg HC/g TOC]
1194.08	Shale	0.00	0.16	0.01	17	0.00	0.03	16	488?	0.00	0.03
1194.50	Shale	0.13	0.17	0.09	2	0.01	0.04	21	487?	0.22	0.05
1194.58	Shale	0.22	0.21	0.04	5	0.01	0.04	19	480?	0.20	0.05
1310.08	Shale	1.23	2.97	0.03	97	0.11	1.52	51	447	0.06	1.62
1310.58	Shale	5.58	3.26	0.08	42	0.11	2.12	65	441	0.05	2.23
1310.80	Shale	4.47	2.89	0.05	59	0.12	1.26	43	444	0.08	1.37
1311.55	Shale	9.05	3.39	0.12	29	0.13	2.78	82	435	0.04	2.91
1312.95	Shale	23.39	10.25	0.48	21	3.31	50.07	488	440	0.06	53.38
1313.37	Shale	14.44	5.31	0.75	7	1.57	20.28	382	440	0.07	21.85
1314.16	Shale	1.50	3.33	0.08	42	0.22	1.99	60	447	0.10	2.21
1314.23	Driftwood	5.13	51.20	1.46	35	5.95	79.12	155	445	0.07	85.07
1316.88	Shale	0.27	1.33	0.07	20	0.05	0.34	26	451	0.12	0.39
1317.25	Shale	0.03	1.51	0.04	42	0.04	0.36	24	442	0.10	0.40
1326.95	Shale	0.67	1.07	0.02	50	0.05	0.29	27	451	0.14	0.33
1327.67	Shale	2.22	1.04	0.04	23	0.04	0.55	53	443	0.07	0.59
1328.10	Shale	5.87	0.95	0.16	6	0.04	0.34	35	441	0.09	0.37
1328.65	Shale	8.31	1.18	0.04	30	0.04	0.58	49	440	0.06	0.62
1328.85	Shale	2.05	1.57	0.03	58	0.13	1.73	110	442	0.07	1.86
1329.35	Shale	0.00	8.44	0.78	11	2.31	34.08	404	439	0.06	36.39
1329.71	Shale	0.02	3.54	0.28	13	0.46	8.11	229	441	0.05	8.56
1330.15	Shale	0.50	2.83	0.17	17	0.31	5.05	178	440	0.06	5.36
1330.70	Shale	0.00	3.35	0.21	16	0.45	8.43	252	440	0.05	8.88
1331.10	Shale	0.19	4.91	0.18	27	0.86	14.20	289	441	0.06	15.06
1331.66	Shale	0.10	4.34	0.56	8	0.69	10.84	250	438	0.06	11.53
1332.43	Shale	0.72	3.62	0.22	16	0.56	8.86	245	439	0.06	9.41
1333.10	Shale	1.17	4.56	0.27	17	0.87	12.48	273	440	0.06	13.35
1333.30	Shale	1.85	4.86	0.26	19	1.02	14.53	299	440	0.07	15.55
1333.85	Shale	0.39	2.92	0.21	14	0.44	6.76	231	440	0.06	7.20
1334.22	Shale	0.31	4.07	0.41	10	0.61	9.88	243	439	0.06	10.49
1334.85	Shale	1.81	3.29	0.13	25	0.57	7.83	238	438	0.07	8.40
1335.30	Shale	0.37	2.44	0.14	17	0.30	5.12	210	441	0.05	5.41
1335.75	Shale	0.09	2.06	0.09	23	0.21	1.82	88	440	0.10	2.03
1336.12	Shale	0.15	4.45	0.29	15	0.80	11.92	268	439	0.06	12.72
1336.90	Shale	0.00	5.35	0.59	9	1.09	15.81	295	439	0.06	16.90
1337.40	Shale	1.25	5.25	0.46	11	1.18	18.46	351	438	0.06	19.64
1338.00	Shale	0.65	7.19	0.72	10	1.73	27.46	382	436	0.06	29.19
1338.35	Shale	18.09	9.89	0.43	23	2.99	47.52	480	441	0.06	50.51
1339.20	Shale	36.54	3.30	0.03	99	0.67	6.93	210	438	0.09	7.60
1341.20	Shale	0.82	3.18	0.04	80	0.26	1.73	54	446	0.13	2.00
1345.00	Shale	0.28	1.23	0.02	63	0.08	0.32	26	460	0.19	0.39
1350.00	Shale	0.88	1.39	0.02	86	0.05	1.27	91	441	0.03	1.31
1350.30	Shale	5.05	1.82	0.11	17	0.11	0.94	52	439	0.10	1.05
1350.70	Shale	7.94	2.41	0.09	28	0.14	4.21	175	439	0.03	4.34
1350.95	Shale	30.69	3.72	0.02	197	0.33	10.84	291	437	0.03	11.16
1358.90	Shale	0.84	2.35	0.03	86	0.14	0.81	34	457	0.15	0.95
1391.00	Shale	0.10	0.13	0.10	1	0.01	0.03	22	442?	0.14	0.04

the depth interval from 1339.20 to 1312.95 m. The correlation between $\delta^{13}C$ values of pristane and phytane is excellent ($r^2 = 0.96$).

- Short chain *n*-alkanes (*n*-$C_{15\text{-}17}$) show a similar depth trend as isoprenoids, although the $\delta^{13}C$ values are more negative at shallow depth.
- $\delta^{13}C$ values of long chain *n*-alkanes (*n*-$C_{27\text{-}29}$) are often very negative (−30 to −31‰). However, a positive isotope excursion to −28‰ occurs in the upper part of the main shale interval (1335.75–1329.35 m).
- *n*-alkanes with intermediate chain lengths (*n*-$C_{18\text{-}25}$) occupy an intermediate position.

5. Discussion

5.1. Thermal maturity

Thermal maturity was deduced using T_{max} values from the entire studied succession and vitrinite reflectance data from the main coal seam and the main shale interval. T_{max} values increase in the depth interval from 1300 to 1850 m from ~440 to 465 °C. Random vitrinite reflectance in the main shale interval (1326.95–1339.20 m) is lower (0.56–0.78 %Rr, avg. 0.66 %Rr) than in the main coal seam (#6; 1585.0–1591.2 m; 0.91–0.95%Rr).

This range of T_{max} and random vitrinite reflectance values agrees well with the increase of vitrinite reflectance in the same depth interval (1300–1850 m) from ~0.70 to 1.15 %Rr (NAGRA, 2002). In the following maturity issues are discussed separately for Carboniferous coals and the Permian lacustrine series.

5.1.1. Carboniferous coal

Cross-plots of bitumen index (BI = 100*S1/TOC), hydrogen index (HI = 100*S2/TOC) and quality index (QI = [100*(S1+S2)/TOC] versus T_{max} provide information on the petroleum potential and maturity of coal samples (Fig. 16, Sykes and Snowdon, 2002). According to these plots, the coals from the main seam (#6) reached maturity values close to the onset of gas generation. These data agree well with vitrinite reflectance measured for this seam (0.91–0.95 %Rr; this study; 0.86–0.91 %Rr; NAGRA, 2002). Gas generation already occurred in deeper coal samples (1620–1740 m) where vitrinite reflectance is 0.91–1.03 %Rr according to NAGRA (2002).

In contrast to vitrinite reflectance and T_{max}, biomarker parameters suggest lower maturity for the main seam (#6). For example, MPI-1

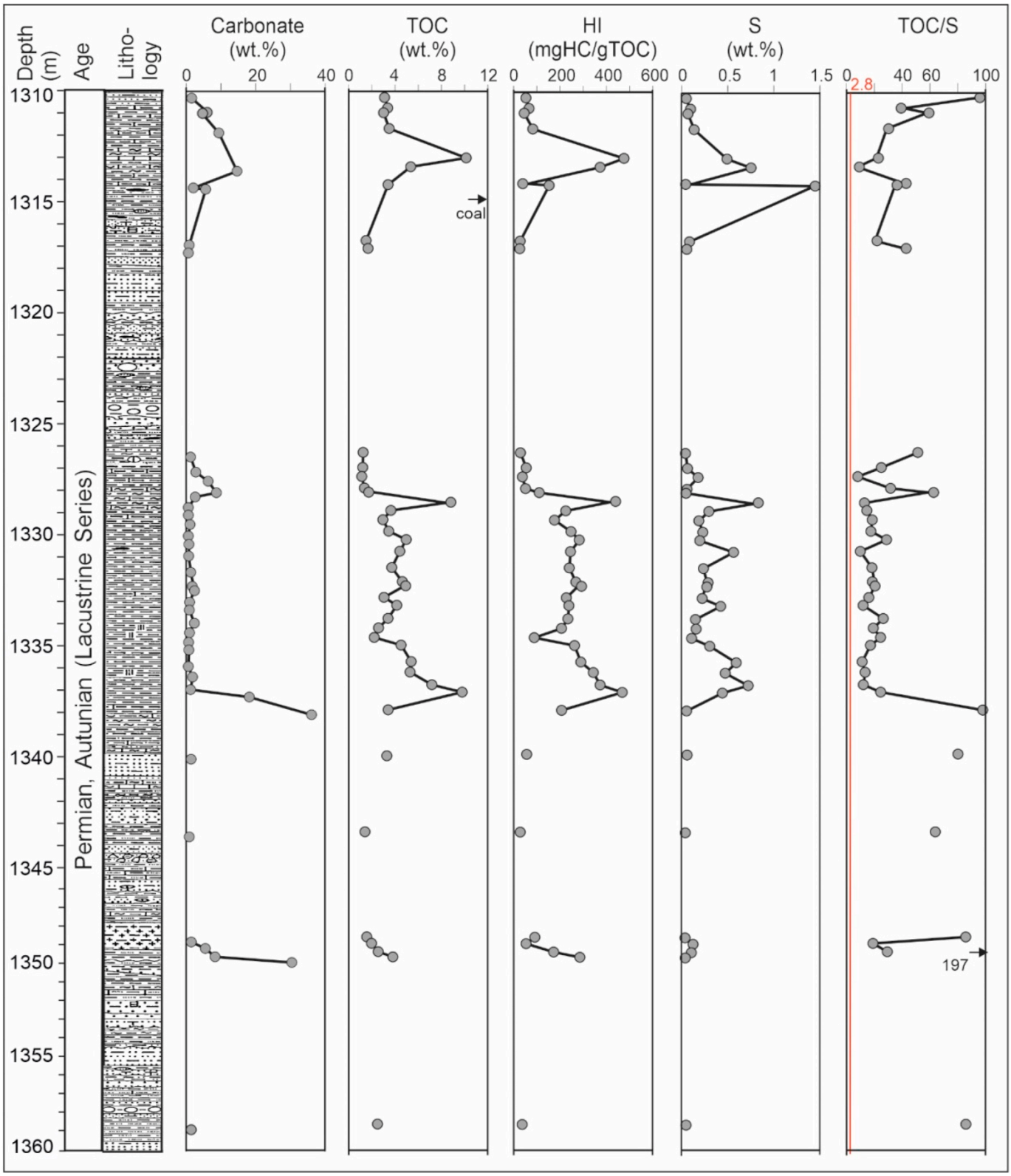

Fig. 9. Depth *versus* bulk geochemical parameters for the Permian lacustrine shales.

values (0.49–0.56) suggest 0.69–0.74% $Rc_{(MPI\ 1)}$ (Radke and Welte, 1983). This maturity corresponds to the maturity of the lacustrine shale unit. However, downward migration (or upward migration from low-maturity deeper shales) is considered unlikely.

5.1.2. Permian Lacustrine Series

T_{max} values of samples from the lacustrine series (1252–1388 m) with $S_2 > 1.0$ mgHC/gTOC (435–447 °C; avg. 440 °C) and vitrinite reflectance of samples between 1310 and 1339 m depth (avg. 0.66 %Rr) suggest early oil window maturity. An average PI of 0.07 shows that major oil generation did not yet start in the Lacustrine Series.

Table 6
Palynofacies, maceral percentages and vitrinite reflectance of samples from the Permian Lacustrine Series. Std – standard deviation, n – number of measurements.

Sample	Palynofacies								Macerals						VR	Std.	n
ID[m]	Orange AOM	Grey, rectangular-shape AOM	∑ (AOM)	Opaque Phytoclasts	Translucent Phytoclasts	Palyno-morphs	*Botryococcus algae*	Fungal remains	Vitrinite	Inertinite	Sporinite	Tel-alginite	Lam-alginite	Lipto-detrinite		dev	
	[vol%]	[vol%]	[vol%]	[vol%]	[vol%]	[vol%]	[vol%]	[vol%]	[vol%]	[vol%]	[vol%]	[vol%]	[vol%]	[vol%]	[% Rr]		
1310.08															0.71	0.05	50
1312.95															0.58	0.11	50
1328.65	55.6	0.0	55.6	19.0	6.5	17.8	0.7	0.4	43	10	0	37	3	7	0.78	0.11	61
1329.35	8.7	68.3	77.0	7.5	4.0	10.5	1.0	0.0	16	29	0	41	5	11			
1330.15	64.0	0.0	64.0	23.3	5.4	6.0	0.0	0.5	18	20	0	25	16	22			
1331.10	60.4	0.0	60.4	14.2	14.0	11.0	0.2	0.2	12	22	1	36	8	21			
1332.43	68.4	0.0	68.4	11.6	8.2	11.8	0.0	0.0	12	8	0	23	5	51			
1333.30	63.7	7.9	71.6	11.0	10.4	6.0	0.0	1.0	41	28	1	25	0	5			
1334.22	8.0	63.5	71.5	8.7	8.3	11.2	0.0	0.3	27	18	0	16	11	28	0.56	0.19	50
1335.75	62.9	0.0	62.9	16.0	2.3	18.5	0.0	0.3	5	48	1	13	12	21			
1336.12	3.6	83.5	87.1	6.3	1.5	4.5	0.4	0.2	18	31	0	22	7	21			
1337.40	7.4	58.2	65.6	9.9	2.2	22.0	0.1	0.2	16	22	0	23	17	22			
1338.35	0.0	97.6	97.6	1.4	0.5	0.5	0.0	0.0	18	41	0	21	16	3	0.63	0.11	50
1339.20	44.0	23.3	67.3	20.1	5.5	6.8	0.1	0.2	19	63	0	16	0	2			

Fig. 10. Photomicrographs of maceral composition of selected samples (Left: white light; right: fluorescent mode).

Biomarker maturity parameters show strong vertical variations and are probably influenced by facies variations. However, average values generally support early oil window maturity. For example the average MPI-1 value (0.44) suggests an average vitrinite reflectance of 0.66% $Rc_{(MPI\ 1)}$ (Radke and Welte, 1983).

5.2. Hydrocarbon source potential

5.2.1. Carboniferous coal measures

The plot of hydrogen index versus T_{max} (Fig. 16b) suggests that the coals are mainly gas prone, but may also generate minor amounts of oil. However, low percentages of liptinite macerals (avg. 3.7 vol%; Table 2) and relatively high percentages of inertinite macerals (up to 14 vol%) indicate that the oil potential is limited. Surprisingly, a strong positive correlation ($r^2 = 0.93$) exists between vitrinite macerals and HI. This suggests that HI may be controlled by hydrogen-rich substances adsorbed in the vitrinite matrix. Similarly, Wolf et al. (1988) noted a

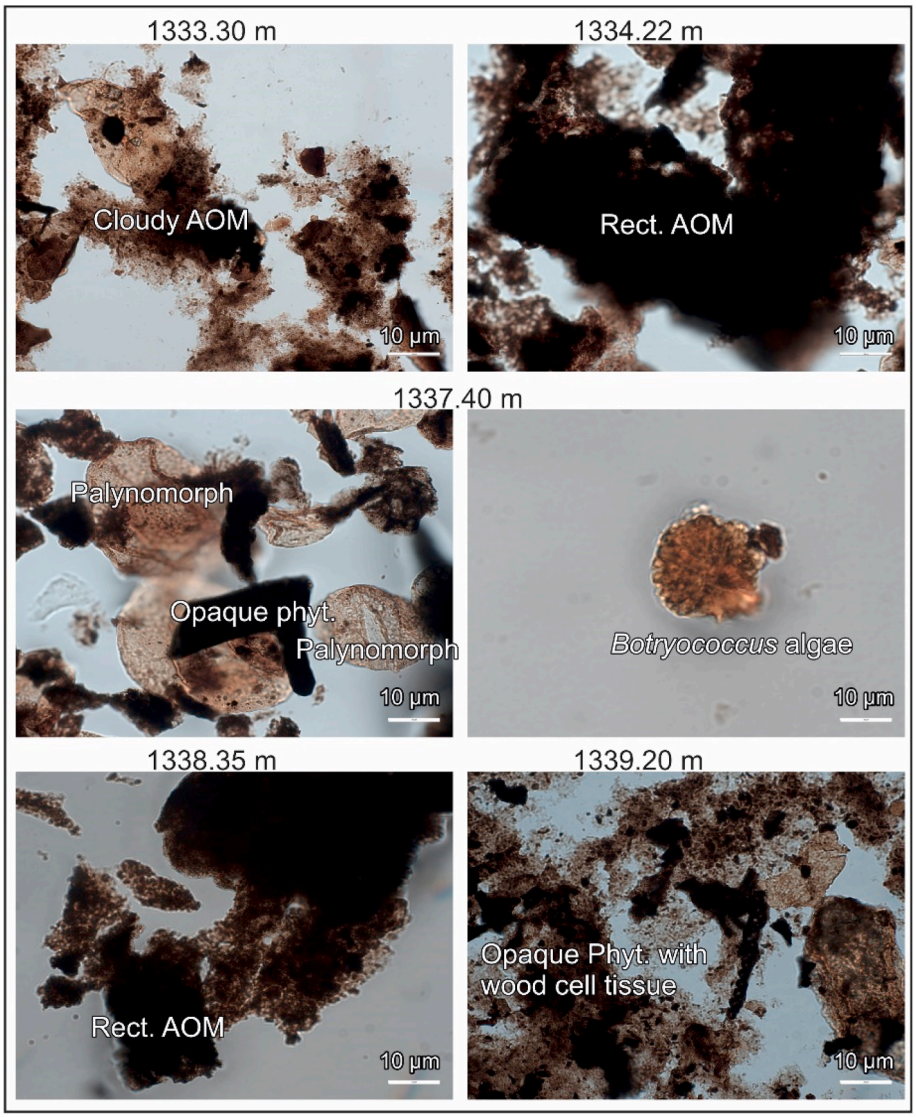

Fig. 11. Photomicrographs of palynofacies for selected samples from the main shale interval in the Lacustrine Series.

relatively high hydrogen content of the Weiach coals and assumed that this is due to secondary bitumen impregnations. As noted, based on HI, generation of minor amounts of liquid hydrocarbons cannot be excluded. The Upper Carboniferous coals are the most likely source rock for the Entlebuch gas field beneath the Molasse sediments (Vollmayr and Wendt, 1987; Leu, 2012) and the gas found at great depth during the drilling of the geothermal St. Gallen GT-1 well (Omodeo-Salé et al., 2020 and references). This shows that the knowledge of deeply buried Carboniferous rocks is important for eventual future hydrocarbon exploration in northern Switzerland (e.g., Leu, 2012), but also to derisk the geothermal exploration activity (Omodeo-Salé et al., 2020).

Carboniferous shales have been described as bituminous (e.g. Matter, 1987; Diebold, 1988). However, based on S_2 and HI values the organic matter in all investigated samples is classified as Type III kerogen (Fig. 2). Hence, these shales are coaly rather than bituminous. Consequently, these samples may hold some additional gas potential, but no oil potential.

5.2.2. *Permian Lacustrine Series*

Shales near the base and the top of the lacustrine series with TOC contents below 0.25 wt% do not hold any hydrocarbon potential. The following discussion therefore focuses on the depth range between 1358.90 and 1310.08 m, where TOC contents are significantly higher (0.95–10.25 wt%). For these samples, the plots of S_2 against TOC for different depth intervals are shown separately in Fig. 17. The interval between 1358.90 and 1341.20 m contains mainly Type III kerogen, but a single sample is classified as Type II kerogen (Fig. 4a).

The plot for samples from the main shale interval (1339.20–1326.95 m; Fig. 17b) shows that Type III kerogen predominates in the uppermost part (above 1328.85 m). The remaining samples follow a linear trend in the S_2 versus TOC diagram. The slope and the intercept of the regression line show a high percentage (~2 wt%) of inert carbon (e.g. inertinite, vitrinite) and that the HI of the reactive organic matter is about 550 mgHC/gTOC (cf. Dahl et al., 2004). This indicates the presence of highly oil prone Type II kerogen also in samples with relative low measured HI.

A similar plot for samples from the upper interval shows an even slightly higher amount of inert carbon and a slightly higher HI (685 mgHC/gTOC) of the reactive kerogen (Fig. 17a). However, this plot is based on a low sample number.

Overall, data plotted in Fig. 17 reflects that the organic matter is a mixture of terrigenous and aquatic organic matter (see palynofacies and maceral data; Table 6).

The plot of Petroleum Potential (S_1+S_2) versus TOC (Fig. 18) is often used to quantify the generation potential. It shows that good to very good source rocks exist in the main shale interval, but also in underlying and overlying Permian shale layers.

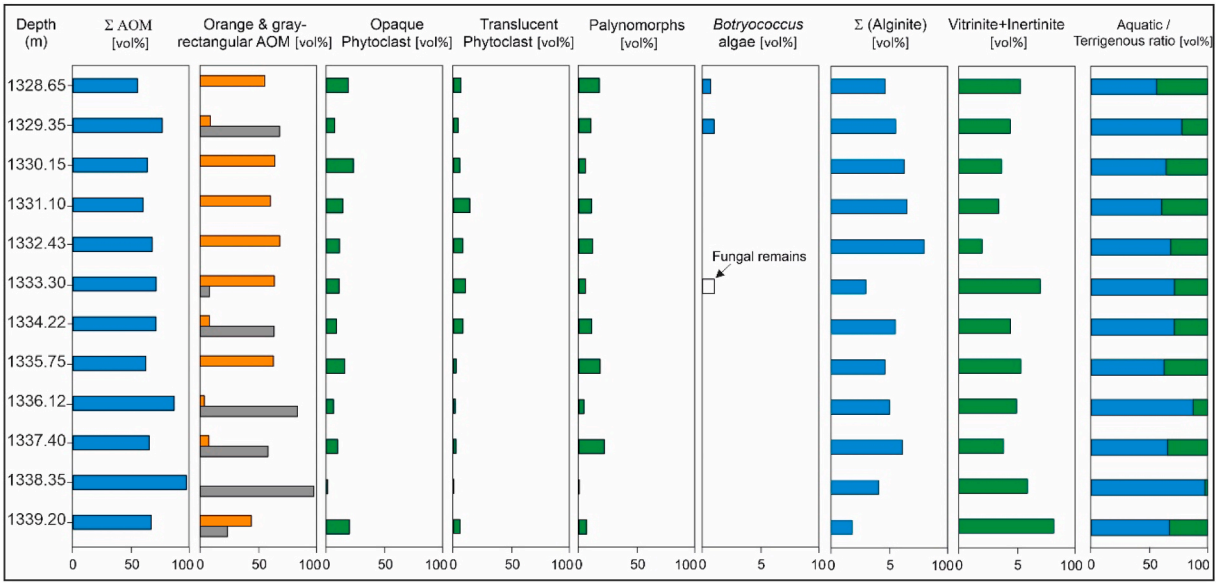

Fig. 12. Depth plot of palynofacies and maceral composition for selected samples from the main lacustrine shale succession. (Aquatic: Σ AOM + Botryococcus; Terrigenous: Phytoclasts + palynomorphs).

The source potential index (SPI=(S1+S2 [mgHC/g rock])*thickness [m]*rock density [g/cm^3]/1000) can be used to quantify the amount of hydrocarbon generated beneath one square meter of surface area (Demaison and Huizinga, 1994). The SPI has been calculated for the 12.25 m thick main shale interval, considering the average petroleum potential (11.92 mgHC/g rock) and an estimated rock density of 2.4 g/cm^3. With these input parameters, the calculation results in a SPI of 0.35 tHC/m^2. However, this value neglects the presence of additional layers with high oil potential in the lacustrine series. Therefore, the total SPI might be higher. Based on the work of Demaison and Huizinga (1994), an SPI of 0.35 tHC/m^2 is classified as low. However, it is equal to the SPI of the Schöneck Formation, the main source rock in the NAFB (Sachsenhofer et al., 2010).

In the eastern (Austrian) and central (German) sectors of the basin, the extension of the Permian succession in the basement of the NAFB is limited, suggesting that the lacustrine series is not a main source rock interval in these parts of the basin. In contrast, the extension in the eastern (Swiss) sector is probably larger, but poorly known. This suggests that Permian lacustrine source rocks may have contributed locally to hydrocarbon accumulations (e.g. Do Couto et al., 2021; Pullan and Berry, 2019).

5.2.3. Possibilites to distinguish oil of Permo-Carboniferous origin

The main source rocks in the NAFB are the Oligocene Schöneck Formation (Schulz et al., 2002; Sachsenhofer and Schulz, 2006; Gratzer et al., 2011; Bechtel et al., 2013) and the Toarcian Posidonia Shale (Littke et al., 1991; Wehner and Kuckelkorn, 1995; Bechtel et al., 2019).

Biomarker ratios and isotope patterns that can help distinguish oil shows derived from Permo-Carboniferous source rocks from those derived from the main Jurassic and Oligocene source rocks are defined below. Box plots summarizing biomarker ratios of Permo-Carboniferous and Jurassic source rock extracts and of oil samples generated from Oligocene source rocks are shown in Fig. 19. In the case of Permian shales, non-source rock samples (S1+S2: <1 mgHC/gTOC) are neglected.

The distinction of Permo-Carboniferous (and Jurassic) oils from oil generated by the Oligocene Schöneck Formation is simple. Unique features of Oligocene-source oils include the presence of considerable amounts of oleanane, a biomarker characteristic for angiosperms which only evolved after the Late Cretaceous (Moldowan et al., 1994) and relatively high C_{28}/C_{29} sterane ratios (~1; Fig. 19) reflecting the young age of the source rock (Grantham and Wakefield, 1988). Moreover, Oligocene source rocks and their oils are characterized by a very specific ("V-shaped") CSI pattern, characterized by very negative $\delta^{13}C$ values of mid-chain *n*-alkanes (especially *n*-C_{21}; -Gratzer et al., 2011; Bechtel et al., 2013).

The Stephanian coals probably will generate only minor amounts of liquid hydrocarbons. Any coal-generated oil, however, should be identified easily based on very high Pr/Ph ratios (3.6–5.0) and very high C_{19}/C_{23} and C_{20}/C_{23} tricyclic terpane ratios (Table 3; Fig. 19).

Permian lacustrine and Lower Jurassic marine source rocks contain comparable Pr/Ph ratios and sterane distributions and display similar CSI patterns (e.g., Ajuaba et al., 2022). However, a distinction of Permian oils should be possible based on the fact that Permian rock extracts contain significantly higher amounts of tricyclic terpenates (TT; tricyclic terpenates/hopanes ratio) and higher ratios of C_{19}/C_{23} TT (avg. 1.16) and C_{20}/C_{23} TT ratios (1.8) than Posidonia Shale extracts (0.06 and 0.22, respectively; Fig. 19). Moreover, the C_{30} diahopane/hopane ratio is significantly higher for Permian extracts (0.29) than for Jurassic extracts (0.06). Finally, the sterane/hopane ratio is lower in Permian rocks extracts (0.20 on average) than in Jurassic ones (3.69 on average; Fig. 19).

5.3. Implications of study results for the reconstruction of the depositional environment

The results presented in this work provide indications on the depositional environment of the main coal seam in the Carboniferous succession and the Permian lacustrine deposits.

5.3.1. Carboniferous coal measures

The lithological log of the main seam (#6) is shown in Fig. 3 after Wolf et al. (1988) and Matter et al. (1988). The seam overlies laminated fine-grained, shaly sandstone. It contains relatively clean coal in the lower part (10 wt% ash, db) with ash yields increasing upwards to 46 wt %db (Fig. 3b). High ash yields are reflected by low TOC contents (77.0–35.5 wt%; Fig. 3b). Based on the absence of rooted horizons and high mineral matter contents, Wolf et al. (1988) assumed an hypautochthonous to allochthonous origin of the coal seams. High ash yields together with low sulphur contents (<0.5 wt% in the main seam; Fig. 3c; <0.9 wt% in other seams) support an origin in a non-marine low-lying mire. A thick tuff and several thin (1–30 mm) tonstein layers occur in the

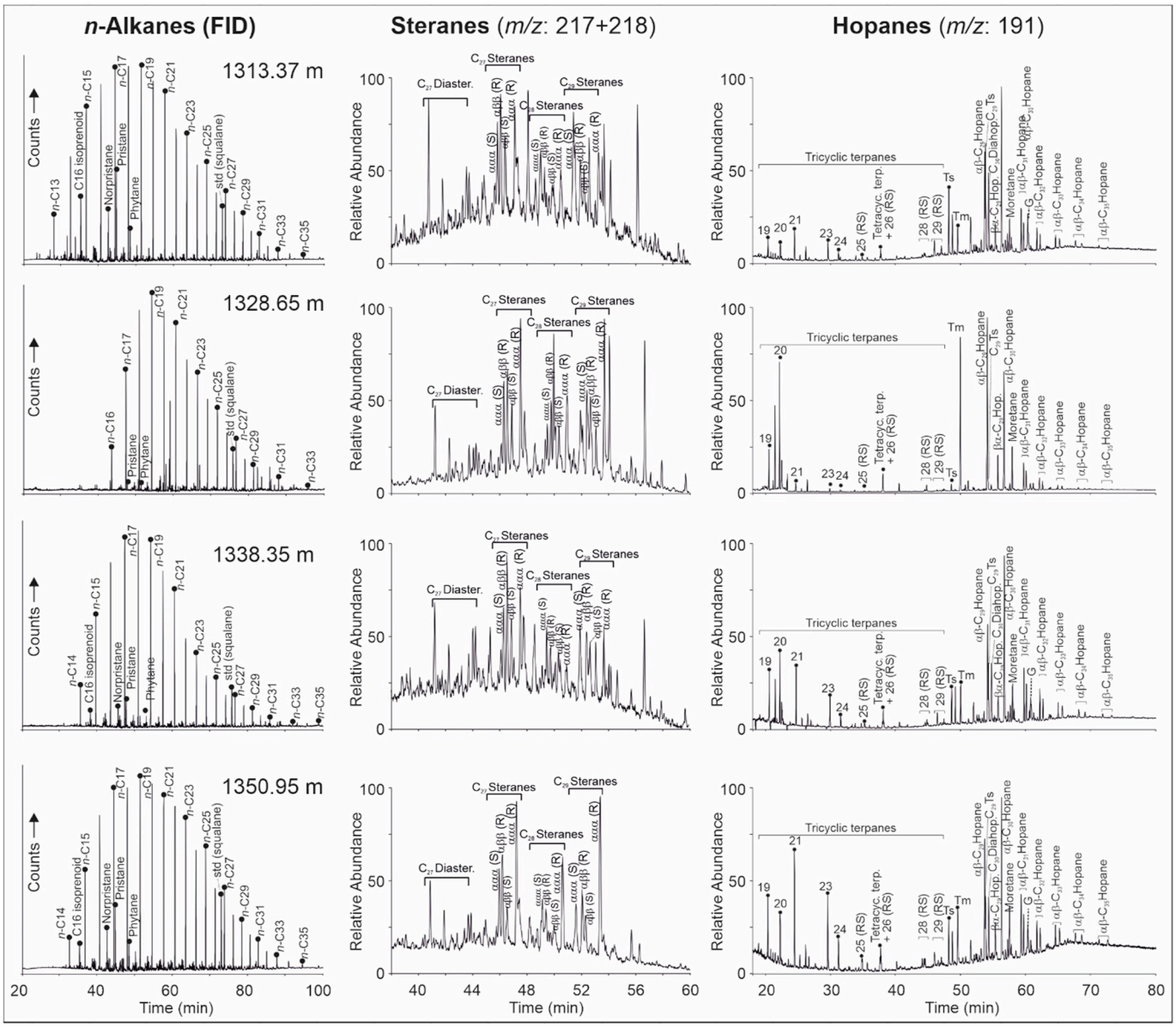

Fig. 13. Mass chromatograms of selected shale samples from the Permian Lacustrine Series.

seam (Wolf et al., 1988) and reflect strong contemporary volcanic activity, whereas alteration to kaolinite testifies to acidic conditions.

The top of the seam (1585.01 m) is overlain by cross-bedded conglomeratic sandstones, several metres thick (Matter et al., 1988). The presence of coaly shales and shales in the upper part of the seam and the lithology of the overlying rocks suggest that peat accumulation ended due to channel(s) avulsion.

A detailed petrographic study using polished blocks of 120 samples was performed by Wolf et al. (1988). They reported a relatively high percentage of inertinite (17 vol%) and low percentage of liptinite macerals (3 vol%). Although only six samples were investigated in the present study, the overall results are similar (inertinite: 11 vol%; liptinite: 4 vol%). Despite the low liptinite contents, Wolf et al. (1988) noted that the coal samples are relatively rich in hydrogen (5.3 wt%$_{daf}$) and concluded that this is due to secondary bitumen. In agreement with this observation, HI values are also relatively high and not related to liptinite contents. Alternatively, HI may be enhanced due to migration of hydrocarbons from adjacent shale source beds (see section 5.1.1).

Geochemical parameters are within the range expected for coal samples. High Pr/Ph ratios (3.6–5.0) and high amounts of C_{29} steranes (44–58 wt%) reflect the predominant input of land-plants. Very low sterane/hopane ratios (≤0.15; Table 3) indicate high bacteria activity, characteristic for many peat-forming environments (Dai et al., 2020). High concentrations of hopanoids in these environments have been related to wood-degrading bacteria (e.g. Bechtel et al., 2007a,b, 2008).

5.3.2. *Lacustrine series*

The postulated lacustrine setting is evidenced by low sulphur contents and high TOC/S ratios (Table 5, Fig. 9). This is also supported by the regular occurrence of the freshwater to brackish water algae *Botryococcus*, albeit in trace amounts, and the absence of any marine organic particles, like dinoflagellate cysts or foraminifer linings.

The most detailed information is available for the main shale interval, which can be subdivided into a lower organic matter-rich part (1339.20–1329.35 m) and a thin, less organic matter-rich upper part (1328.85–1326.95 m; Fig. 9). The organic material of the lower organic matter-rich part is dominated by aquatic organisms, as shown by the prevailing Type II kerogen (Fig. 4; 17b) and high concentrations of short-chain *n*-alkanes (Fig. 14a) and C_{27} steranes (Fig. 14b). The Pr/Ph ratio is a widely used redox parameter (e.g. Didyk et al., 1978).

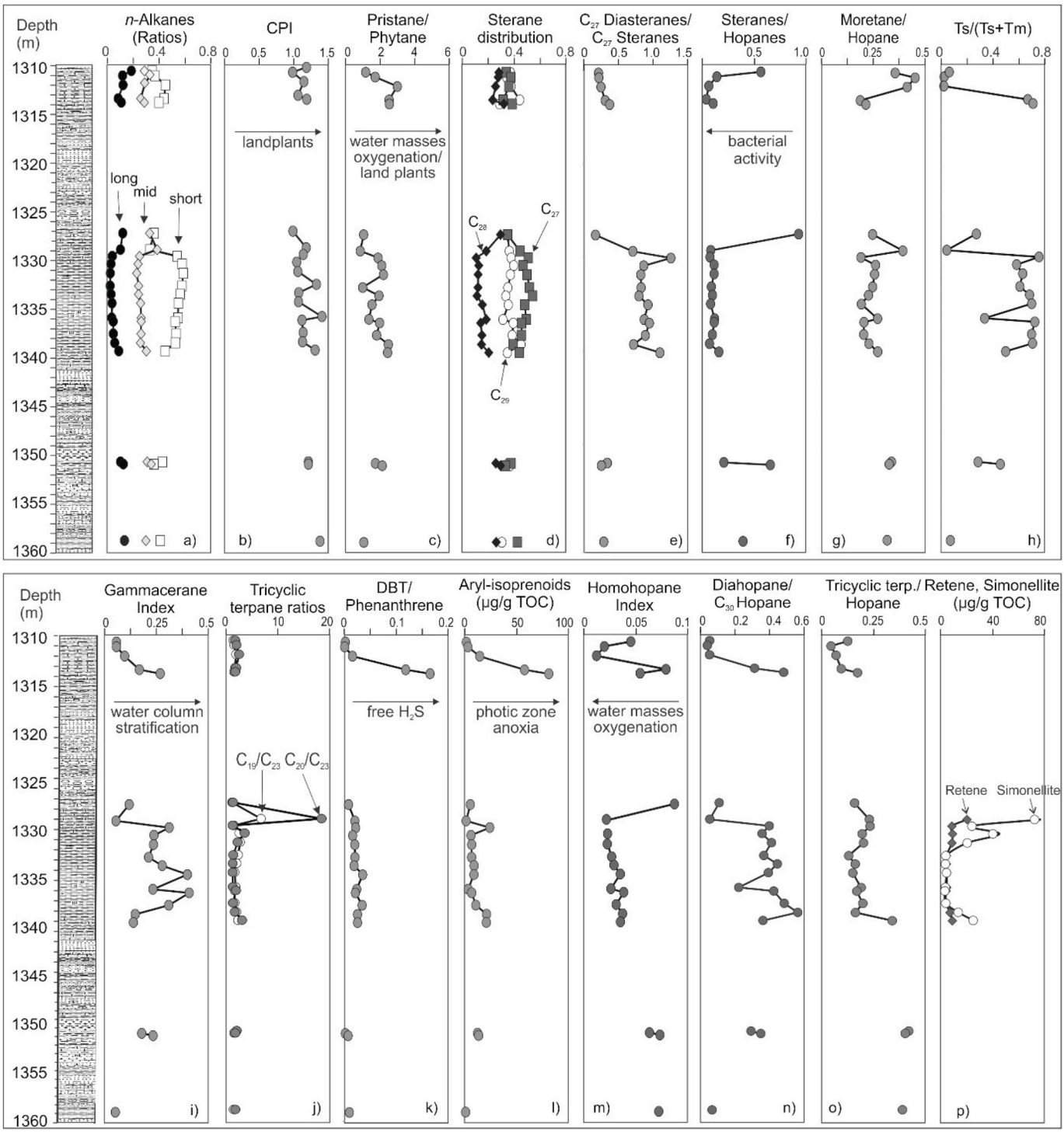

Fig. 14. Concentrations and ratios of selected organic compounds (a–p). Alkane distribution: short-chain: *n*-$C_{15\text{-}19}$/Σ*n*-alkanes; mid-chain: *n*-$C_{21\text{-}25}$/Σ*n*-alkanes; long-chain: *n*-$C_{27\text{-}31}$/Σ*n*-alkanes; CPI: Carbon Preference Index (Bray and Evans, 1961), sterane distribution: $C_{27}/C_{27\text{-}29}$ steranes, $C_{28}/C_{27\text{-}29}$ steranes, $C_{29}/C_{27\text{-}29}$ steranes; DBT: dibenzothiophene.

However, in the present case, the good correlation between Pr/Ph ratio and CPI (cf. Fig. 14b and c) suggests that the Pr/Ph ratio is mainly controlled by the input of land-plants rather than by oxygen availability. Hence, the concentration of aryl-isoprenoids (Fig. 14l) and the homohopane index (HHI; Fig. 14m) may be the better redox proxies. Both parameters indicate strongly anoxic conditions and probably even photic zone anoxia during the early stage of shale deposition followed by gradually increasing oxygen availability. Apart from the main shale interval, strongly anoxic conditions also occurred during deposition of the sediments at about 1314 m depth (Fig. 14l and m).

Vertical trends of the gammacerane index (Fig. 14i) suggest that oxygen restriction was caused by water column stratification. A low energy environment is a prerequisite for water column stratification. Preservation of delicate biological structures observed in several opaque phytoclasts is an additional indication of a low-energy setting. As expected in a lacustrine environment, the availability of free H_2S was very low as suggested by low DBT/Phenanthrene ratios (Fig. 14k). Despite of the generally low values, the DBT/Phenanthrene ratios (Fig. 14k) show

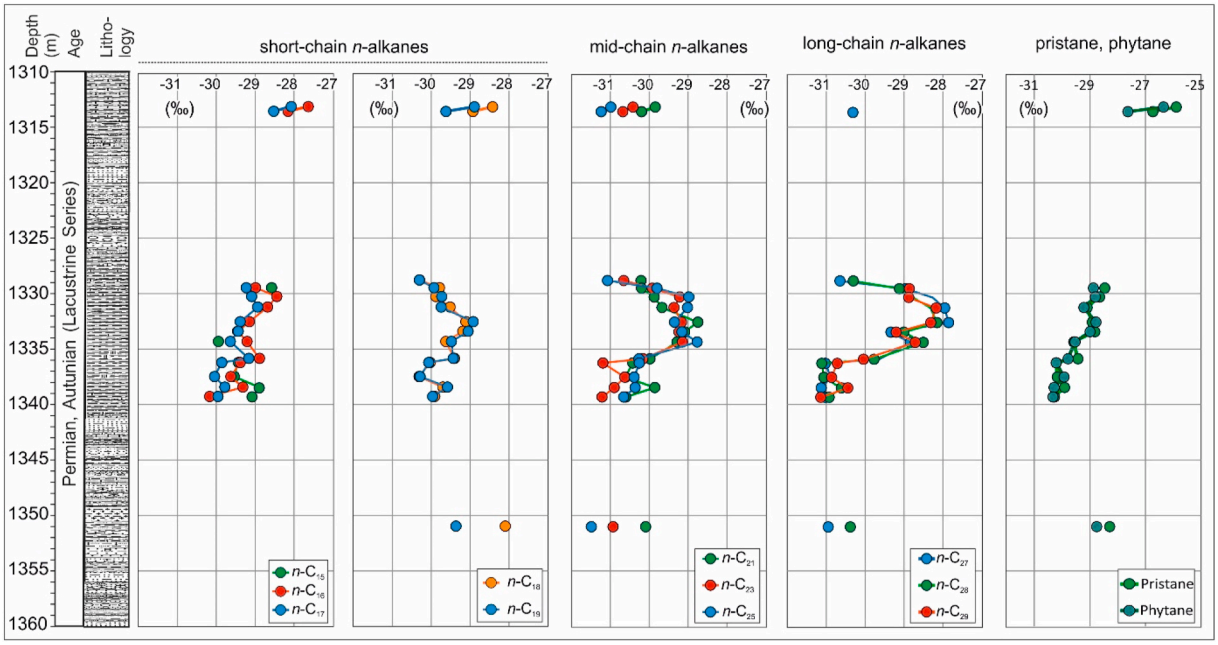

Fig. 15. Vertical variation of $\delta^{13}C$ values of *n*-alkanes, pristane and phytane.

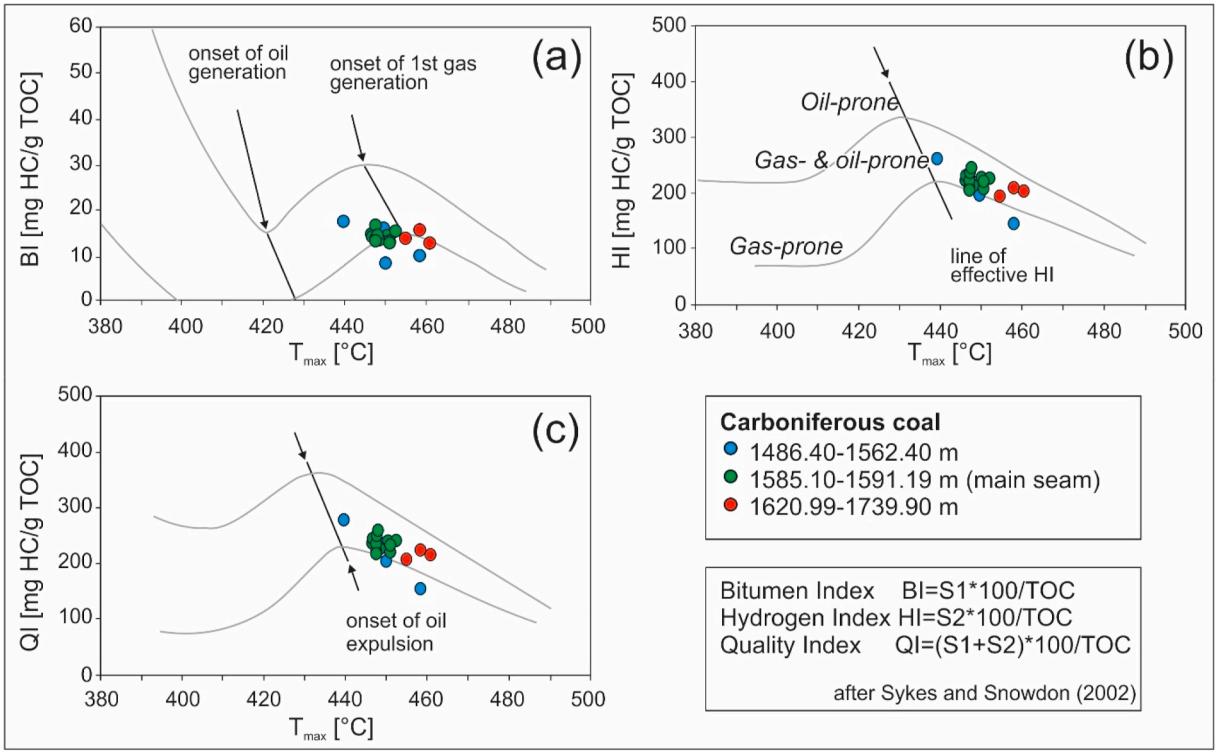

Fig. 16. Cross-plots of T_{max} versus (a) bitumen index (BI), (b) hydrogen index (HI), and (c) quality index (QI) for the interpretation of Rock-Eval data from coals (according to Sykes and Snowdon, 2002).

similar depth trends as the other redox parameters. With few exceptions, the sterane/hopane is below 0.2 indicating high bacterial activity (Fig. 14f). At least partly, high concentrations of hopanes are related to bacteria degrading plant tissues in terrigenous environments (Bechtel et al., 2007a, 2007b).

Additional insight into the origin of organic matter is provided by palynofacies data, especially by the abundance of different types of AOM. Proportions of rectangular AOM show a moderate positive correlation between HI and TOC (r^2 = 0.50 and 0.59, respectively), while proportions of orange, cloudy AOM shows moderate to weak negative correlations (r^2 = 0.51 and 0.40, respectively) (Fig. 20). This suggests that a large part of the organic productivity in the lake facies from Weiach-1 was associated with the rectangular AOM source, while production of the orange, cloudy AOM was associated with reduced paleoproductivity levels in the lake and/or increased oxygen availability.

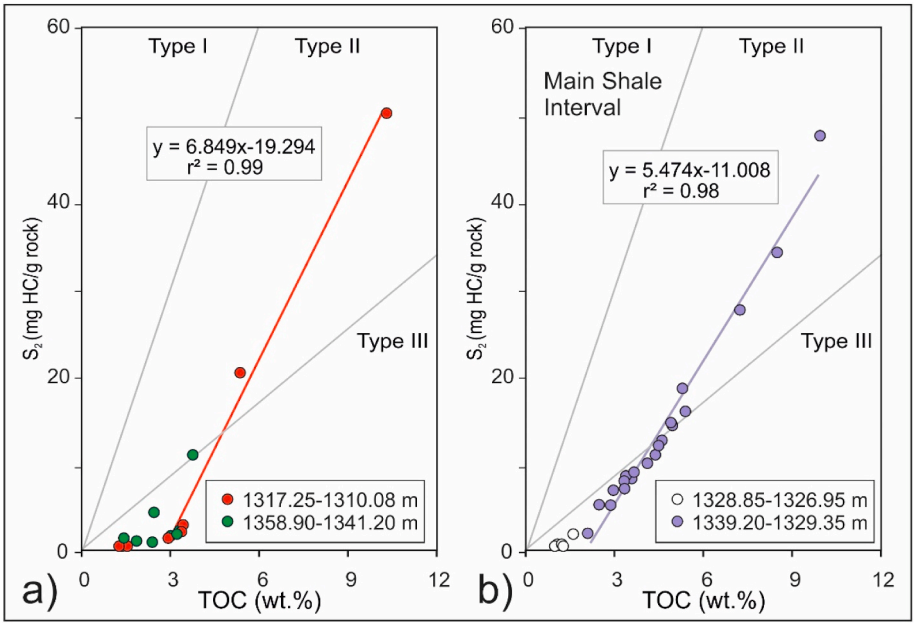

Fig. 17. Plots of S_2 against TOC for the lacustrine series. a) Samples from the lower depth interval (1358.90–1341.20 m) and upper depth interval (1317.25–1310.08 m); b) samples from the main shale interval (1339.20–1326.95 m). Regression lines are shown for samples with TOC contents >2 wt% from the upper depth interval and the main shale interval in order to determine the amount of inert kerogen and the HI of reactive organic matter (see Dahl et al., 2004).

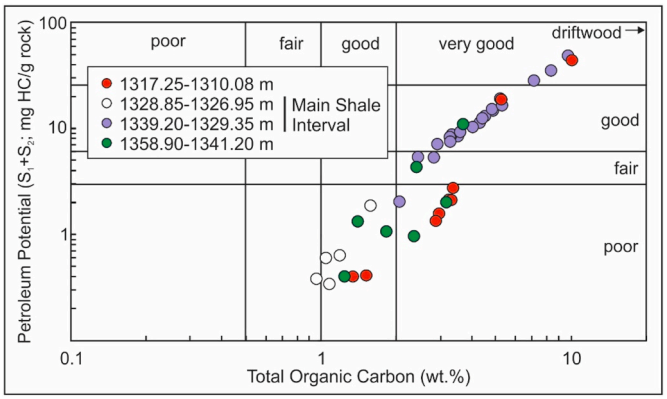

Fig. 18. Plot of petroleum potential (Rock-Eval S1+S2) versus total organic carbon for samples from the Permian lacustrine series.

Sub-rectangular AOM is known to be formed in peat and marsh environments through amorphization and gelification processes in low-energy locations (Laggoun-Défarge et al., 1999; Sebag et al., 2006; Garel et al., 2013; Storme et al., 2012) and, therefore, our results suggest the greater occurrence of such paleoenvironmetal conditions between 1339.20 m and 1334.22 m. These paleoenvironmental conditions seem to have been the most favourable for organic production and preservation in the Weiach-1 core. The exact nature of the higher plants sources leading to the sub-rectangular AOM are not known in Weiach-1. Based on the high amount of short-chain *n*-alkanes and C_{27} steranes, the sub-rectangular AOM are probably not related to emerged land-plants in vegetated areas at the boarders parts of the lake system. In contrast, submerged (or floating) aquatic plants are a more likely source.

From 1333.30 to 1328.65 m, the increasing proportions of orange, cloudy AOM in palynofacies suggest enhanced algal/bacterial surface production, however associated with lower organic fluxes as TOC and HI values are lower than between 1339.20 m up to 1334.22 m. The lake system may have been more open and enlarged, possibly deeper, favoring surface algal/bacterial productivity in the photic waters of the lake.

5.3.3. Stable carbon isotope data in Permo-Carboniferous terrigenous environments

5.3.3.1. Main coal seam. Carbon and nitrogen isotope data from coals and black shales in the Permo-Carboniferous Igornay and Muse formations in the Autun Basin (Massif Central) have been reported recently by Mercuzot et al. (2021). They observed background $\delta^{13}C$ values of aquatic and dispersed terrigenous organic matter of around −23.5‰ and −20.0‰, respectively, and of coal of around −24 to −25‰. These data can be compared with the compound-specific stable carbon isotope data from the coeval coal series and the lacustrine series.

The average $\delta^{13}C$ value of long-chain *n*-alkanes (*n*-C_{25-29}; −27.6‰) and isoprenoids (−27.4‰) in the coal samples is slightly more negative than bulk ^{13}C values of the coeval coals in the Autun Basin. The difference (~3‰) is about the same as that observed between coal and the saturated hydrocarbon fraction for Carboniferous coals in Poland (Kotarba and Clayton, 2003). Hence, the bulk coal data from the Massif Central and the CSI data from Weiach match well. They also agree with isotope data from Upper Carboniferous coal samples in other parts of the world (Peters-Kottig et al., 2006; Zdravkov et al., 2017). A clear vertical trend of $\delta^{13}C$ values, which may reflect temporal changes in atmospheric CO_2, is neither expected nor observed in the 10-m-thick seam.

5.3.3.2. Lacustrine series. $\delta^{13}C$ values of *n*-alkanes and isoprenoids in the lacustrine series show a larger variability and significant stratigraphic trends (Fig. 15). $\delta^{13}C$ values of pristane and phytane are similar in most samples (difference ≤0.4‰). Although the difference is slightly greater (0.46–0.89‰) in two samples above the main shale interval, this suggests a common chlorophyll precursor and that non-chlorophyll-derived phytane is largely absent (e.g. Aghayeva et al., 2021).

Pristane and phytane show the same stratigraphic $\delta^{13}C$ trend as the short-chain *n*-alkanes *n*-C_{15} and *n*-C_{16}, which are derived mainly from aquatic organisms, including bacteria and algae (Cranwell et al., 1987). In contrast, mid- and long-chain *n*-alkanes, derived at least partly from submergent plants (e.g. Ficken et al., 2000) and land plants (e.g. Eglinton et al., 1962), show different stratigraphic trends (Fig. 15). This suggests that pristane and phytane are derived from the chlorophyll of aquatic plants. Consequently, the uniform upward increase in $\delta^{13}C$

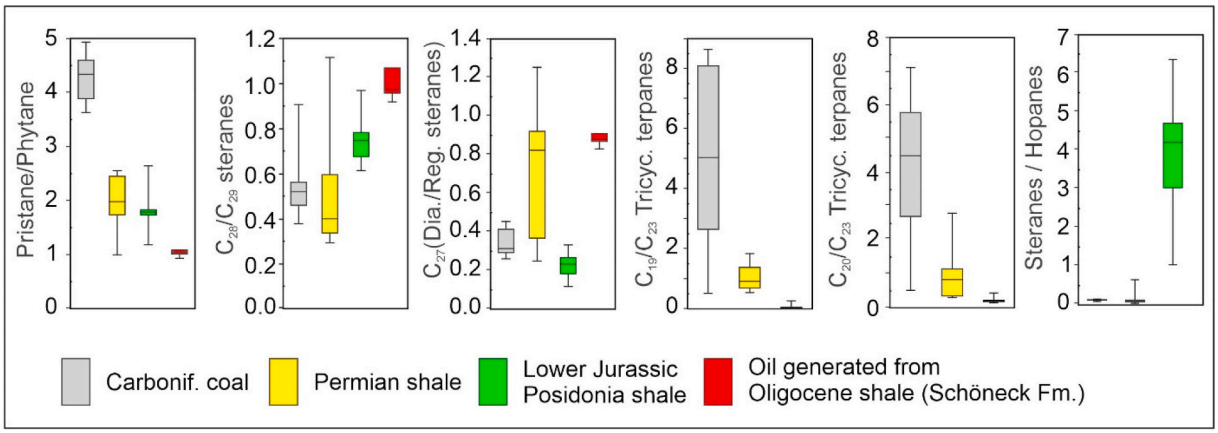

Fig. 19. Box plots (statistical representation from bottom to top are: minimum, first quartile, median, second quartile and maximum) showing distributions of biomarker ratios in extracts from Carboniferous coals (main seam #6; this study), Permian shales (main shale interval; this study), and Toarcian (Lower Jurassic Posidonia shale; Ajuaba et al., 2022). Biomarker ratios of oil samples from the Austrian sector of the NAFB, generated by Oligocene source rocks are shown for comparison (data from Gratzer et al., 2011).

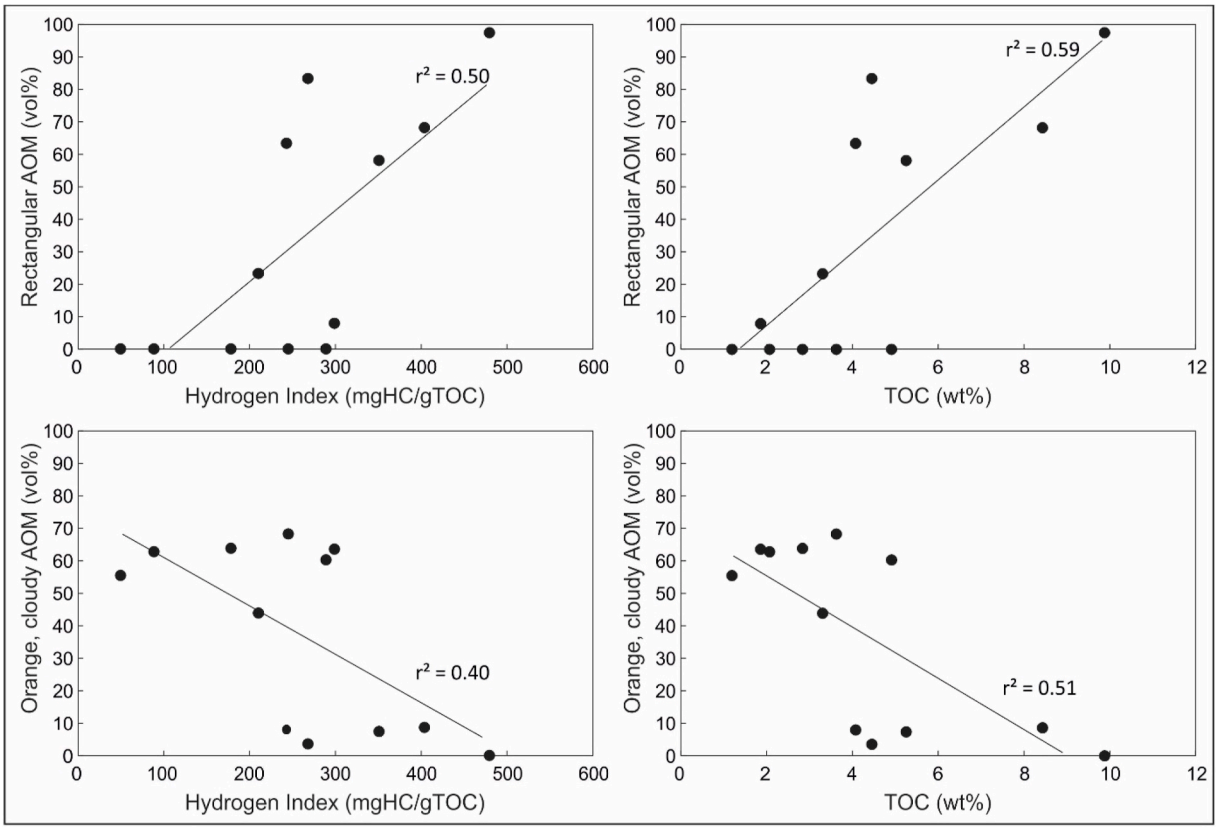

Fig. 20. Plots of the amount of rectangular and orange, cloudy amorphous organic matter (AOM) against hydrogen index and TOC. Percentages of rectangular AOM shows moderate positive correlations, while cloudy AOM shows moderate negative correlations.

values of pristane and phytane reflects a change in the isotopic composition within the water column. The most negative $\delta^{13}C$ values of pristane and phytane (−30.3‰) are observed at the base of the main shale interval (1339.20 m). Based on the amount of aryl-isoprenoids (Fig. 10m) and the homohopane index (HHI; Fig. 10n), this level corresponds to the most anoxic part of the main shale interval. While various factors, like climatic variations or productivity, may affect the lacustrine carbon reservoir, the observed very negative $\delta^{13}C$ values are probably related to remineralization of organic matter in the anoxic water column beneath a strong chemocline (e.g. Küspert, 1982; Jenkyns, 1985; Hayes, 2001). Similarly, Mercuzot et al. (2021) observed strong negative bulk organic carbon excursions in coeval black shales from the Autun Basin. In addition, these authors noted a positive nitrogen isotope excursion in these intervals indicating denitrification and anammox processes. An upward increase in oxygen availability within the main shale interval and a trend towards less negative $\delta^{13}C$ values (Fig. 15) may reflect a weakening of water column stratification, which is also supported by the gammacerane index (Fig. 10i). Mid- and long-chain *n*-alkanes with relatively high $\delta^{13}C$ values probably reflect terrigenous input.

$\delta^{13}C$ values of pristane and phytane in organic-rich layers above the main shale interval (1313.37-1312-95 m) are relatively high (about −26‰; Fig. 15), despite partly strictly anoxic conditions. Apparently, the effect of recycling of isotopically light dissolved inorganic carbon from deeper levels of the stratified water body was limited during deposition of the younger layer.

Whereas pristane and phytane are derived from chlorophyll, short-chain *n*-alkanes (*n*-C_{15-17}) are produced by primary producers (algae, cyanobacteria) and heterotrophs. Consequently, their $\delta^{13}C$ values represent a weighted average of these (Grice et al., 2005). If derived from primary producers, short-chain *n*-alkanes should be depleted in ^{13}C compared with the co-occurring isoprenoids by 1.5‰ (Schouten et al., 1998; Hayes, 2001; Grice et al., 2005). In contrast, enrichment in ^{13}C result from heterotrophic processing of primary photosynthate or dominant contribution of isotopically heavy bacterial biomass (Grice et al., 2005; Fox et al., 2020). In the main shale interval, $\delta^{13}C$ values of short-chain *n*-alkanes and of pristane and phytane are similar (difference <0.8‰). In contrast, $\delta^{13}C$ values of short-chain *n*-alkanes in organic-rich layers above the main shale interval are 1.1–1.7‰ more negative. This suggests that short-chain *n*-alkanes in the upper layer are mainly derived from primary producers, whereas both auto- and heterotrophs contributed to the short-chain *n*-alkanes in the main shale layer.

4. Conclusion

A total of 90 core samples from the Weiach-1 well, located in the Permo-Carboniferous Constance-Frick-Trough beneath the Northern Alpine Foreland Basin (NAFB; Northern Switzerland), have been investigated to study the petroleum potential of coals and shales and to contribute to the understanding of the depositional environment of the main Carboniferous coal seam and the main Permian (Autunian) shale horizon. The most relevant findings of the detailed petrographic and geochemical investigation are summarized below.

- Carboniferous coaly shales, classified as bituminous in earlier studies, do not hold a significant hydrocarbon potential, despite relatively high TOC contents.
- Coals in the Carboniferous coal series are potential source rocks for natural gas. The maturity of the coal series reached the onset of gas generation. The coal would have generated only very limited amounts of oil, which could be identified easily based on biomarker ratios (e.g., high Pr/Ph ratios).
- The petroleum potential of shales in the Permian lacustrine series varies considerably. While some intervals do not exhibit a petroleum potential (TOC <0.3 wt%), bituminous shales in the “main shale interval” (1339.20–1326.95 m) contain very high amounts of organic matter TOC (max. 10.3 wt% TOC) with a high HI (max. 488 mgHC/gTOC). These sediments display “good” to “very good” oil potential. The calculated SPI (Source Potential Index) suggests that the main shale interval may generate about 0.35 tHC/m^2.
- The lacustrine series is probably not a main source rock interval in the NAFB, but it may have contributed to hydrocarbon accumulations. A clear distinction of oil generated from Permian, Jurassic and Oligocene source rocks is possible based on biomarker ratios and CSI data.
- The main seam (#6) was deposited in a low-lying, freshwater mire. Upward increasing mineral matter contents are probably due to delta channel(s) avulsion process in a floodplain setting. Biomarker ratios reflect the high amount of terrigenous organic matter.
- The non-marine environment of the lacustrine series is supported by the presence of the freshwater algae *Botryococcus* and very high TOC/S ratios throughout the main shale interval. The organic matter is mainly of aquatic (algal) origin but with a significant terrigenous input. Bacterial activity was high. Biomarker and palynofacies data show a strongly oxygen-depleted depositional environment, controlled by water column stratification, which even caused photic zone anoxia, and associated with a low energy environment as supported by palynofacies data. In the study interval, these environmental conditions, then changed to a more oxygenated, less stratified and probably deeper and more open lacustrine environment.
- $\delta^{13}C$ values of pristane and phytane in the main shale interval reflect anoxic conditions and remineralization of organic matter.

Author contributions

SA, RFS and DG contributed to the study conception and design. SA, VM and SOS prepared the samples. SA performed the analysis and interpreted the data in collaboration with VM. JS performed part of the analysis and interpreted the corresponding data. RFS, VM, DG, JS, SOS, AM, and DM, helped interpret the entire data. SA wrote the first draft of the manuscript and all authors commented on previous versions of the manuscript. All authors read and approved the final manuscript.

Funding

The study was supported in the frame of the UNCONGEO project (University of Geneva).

Code availability

Not applicable.

Declarations

Conflict of interest

All authors declare that they have no conflict of interest.

Ethics approval

Not applicable.

Consent to participate

Not applicable.

Consent for publication

Not applicable.

Declaration of competing interest

The authors declare that they have no known competing financial interests or personal relationships that could have appeared to influence the work reported in this paper.

Data availability

Data will be made available on request.

Acknowledgments

The authors thank SwissTopo for the permission to take core samples from the Weiach-1 well, at the SwissTopo core shed located in Hochdorf (Switzerland), in the framework of the UNCONGEO project. The authors also thank François Baudin from Sorbonne University for some rock eval analysis and scientific discussion. Careful reviews by the journal reviewers P. Hackley and B. Katz helped to improve the paper significantly.

References

Aghayeva, V., Sachsenhofer, R.F., van Baak, C.G.C., Bechtel, A., Hoyle, T.M., Selby, D., Shiyanova, N., Vincent, S.J., 2021. New geochemical insights into Cenozoic source rocks in Azerbaijan: implications for petroleum systems in the South Caspian Region. J. Petrol. Geol. 44, 349–384.

Ajuaba, S., Sachsenhofer, R.F., Galasso, F., Bechtel, A., Gross, D., Misch, D., Schneebeli-Hermann, E., 2022. Biomarker and compound-specific isotope records across the Toarcian CIE at the Dormettingen section in SW Germany. Int. J. Earth Sciences 111, 1631–1661. https://doi.org/10.1007/s00531-022-02196-z.

Bachmann, G.H., Müller, M., Weggen, K., 1987. Evolution of the Molasse basin (Germany. Switzerland). Tectonophysics 137, 77–92.

Bechtel, A., Reischenbacher, D., Sachsenhofer, R.F., Gratzer, R., Lücke, A., 2007a. Paleogeography and paleoecology of the upper Miocene Zillingdorf lignite deposit (Austria). Int. J. Coal Geol. 69, 119–143.

Bechtel, A., Hámor-Vidó, M., Sachsenhofer, R.F., Reischenbacher, D., Gratzer, R., Püttmann, W., 2007b. The middle Eocene Márkushegy sub-bituminous coal (Hungary): paleoenvironmental implications from petrographical and geochemical studies. Int. J. Coal Geol. 72, 33–52.

Bechtel, A., Gratzer, R., Sachsenhofer, R.F., Gusterhuber, J., Lücke, A., Püttmann, W., 2008. Biomarker and carbon isotope variation in coal and fossil wood of Central Europe through the Cenozoic. Palaeogeogr. Palaeoclimatol. Palaeoecol. 262, 166–175.

Bechtel, A., Gratzer, R., Linzer, H.-G., Sachsenhofer, R.F., 2013. Influence of migration distance, maturity and facies on the stable isotopic composition of alkanes and on carbazole distributions in oils and source rocks of the Alpine Foreland Basin of Austria. Org. Geochem. 62, 74–85.

Bechtel, A., Berling, M., David, P., Dax, F., Garlichs, T.U., Gratzer, R., Groß, D., Köhler, V., Oriabure, J.E., Sachsenhofer, R.F., 2019. Oil-source correlation in the German Molasse basin. 29th Int. Meeting Org. Geochem. https://doi.org/10.3997/2214-4609.201902720 (IMOG 2019).

Bray, E.E., Evans, E.D., 1961. Distribution of n-paraffins as a clue to recognition of source beds. Geochem. Cosmochim. Acta 22, 2–5. https://doi.org/10.1016/0016-7037(61)90069-2.

Burdige, D.J., 2007. Preservation of organic matter in marine sediments: controls, Mechanisms, and an imbalance in sediment organic carbon budgets? Chem. Rev. 107, 615. Chapman and Hall.

Cervelli, M., 2022. Reservoir sedimentology, mineralogy and chemostratigraphy of a Permo – Carboniferous trough infill in NE Switzerland. In: Implication for Geo-Energy Exploration. MSc Thesis, Departmen of Geosciences, University of Padoue, Italy, p. 118.

Clayton, G., Coquel, R., Doubinger, J., Gueinn, K.J., Loboziak, S., Owen, B., Streel, M., 1977. Carboniferous miospores of Western Europe: illustration and zonation. Meded. Rijks Geol. Dienst 29, 1–71.

Cranwell, P., Eglinton, G., Robinson, N., 1987. Lipids of aquatic organisms as potential contributors to lacustrine sediments—II. Org. Geochem. 11, 513–527.

Dahl, B., Bojesen-Koefoed, J., Holm, A., Justwan, H., Rasmussen, E., Thomsen, E., 2004. A new approach to interpreting Rock-Eval S2 and TOC data for kerogen quality assessment. Org. Geochem. 35, 1461–1477.

Dai, S., Bechtel, A., Eble, C.F., Flores, R.M., French, D., Graham, I.T., Hood, M.M., Hower, J.C., Korasidis, V.A., Moore, T.A., Püttman, W., Wei, Q., Zhao, L., O'Keefe, J. M.K., 2020. Recognition of peat depositional environments in coal: a review. Int. J. Coal Geol. 210, 103383, 67.

Demaison, G., Huizinga, B.J., 1994. Genetic classification of petroleum systems using three factors: charge, migration and entrapment. In: Magoon, L.B., Dow, W.G. (Eds.), The Petroleum System, from Source to Trap, vol. 60. AAPG Memoir, pp. 73–89.

Didyk, B., Simoneit, B., Brassell, S., Eglinton, G., 1978. Organic geochemical indicators of palaeoenvironmental conditions of sedimentation. Nature 272, 216–222.

Diebold, P., 1988. Der Nordschweizer Permokarbon-Trog und die Steinkohlefrage der Nordschweiz. Vierteljahrsschrift der Naturforschenden Gesellschaft Zürich 133/1, 143–174.

Diebold, P., Naef, H., Ammann, M., 1991. Zur Tektonik der zentralen Nordschweiz: interpretation aufgrund regionaler Seismik, Oberflächengeologie und Tiefbohrungen. In: Nagra Tech. Ber. NTB. Nagra, Wettingen, p. 277, 90-04.

Do Couto, D., Garel, S., Moscariello, A., Bou Daher, S., Littke, R., Weniger, P., 2021. Origins of hydrocarbons in the Geneva Basin: insights from oil, gas and source rock organic geochemistry. Swiss J. Geosci. 114 (1), 1–28.

Eglinton, G., Gonzalez, A., Hamilton, R., Raphael, R., 1962. Hydrocarbon constituents of the wax coatings of plant leaves: a taxonomic survey. Phytochemistry 1, 89–102.

Espitalie, J., Madec, M., Tissot, B., Mennig, J.J., Leplat, P., 1977. In: Source Rock Characterization Method for Petroleum Exploration. Offshore Technology Conference. https://doi.org/10.4043/2935-MS.

Ficken, K.J., Li, B., Swain, D., Eglinton, G., 2000. An n-alkane proxy for the sedimentary input of submerged/floating freshwater aquatic macrophytes. Org. Geochem. 31, 745–749. https://doi.org/10.1016/S0146-6380(00)00081-4.

Fox, C.P., Cui, X., Whiteside, J.H., Grice, K., 2020. Molecular and isotopic evidence reveals the end-Triassic carbon isotope excursion is not from massive exogenous light carbon. Proc. Natl. Acad. Sci. USA 117 (48), 30171–30178. https://doi.org/10.1073/pnas.1917661117.

Garel, S., Schnyder, J., Jacob, J., Dupuis, C., Boussafir, M., Le Milbeau, C., Storme, J.-Y., Iakovleva, A., Yans, J., Baudin, F., Fléhoc, C., Quesnel, F., 2013. Paleohydrological and paleoenvironmental changes recorded in terrestrial sediments of the Paleocene–Eocene boundary (Normandy, France). Palaeogeogr. Palaeoclimatol. Palaeoecol. 376, 184–199.

Grantham, P.J., Wakefield, L.L., 1988. Variations in the sterane carbon number distribution of marine source rocks derived crude oils through geological time. Org. Geochem. 12, 61–74.

Gratzer, R., Bechtel, A., Sachsenhofer, R.F., Linzer, H.-G., Reischenbacher, D., Schulz, H.-M., 2011. Oil-oil and oil-source rock correlations in the Alpine Foreland Basin of Austria: insights from biomarker and stable carbon isotope studies. Mar. Petrol. Geol. 28, 1171–1186.

Greber, E., Leu, W., Bernoulli, D., Schumacher, M.E., Wyss, R., 1997. Hydrocarbon provinces in the Swiss Southern Alps—a gas geochemistry and basin modelling study. Mar. Petrol. Geol. 14, 3–25.

Grice, K., Cao, C., Love, G.D., Böttcher, M.E., Twitchett, R.J., Grosjean, E., Summons, R. E., Turgeon, S.C., Dunning, W., Jin, Y., 2005. Photic zone euxinia during the Permian-Triassic superanoxic event. Science 307, 706–709.

Grice, K., de Mesmay, R., Glucina, A., Wang, S., 2008. An improved and rapid 5A molecular sieve method for gas chromatography isotope ratio mass spectrometry of n-alkanes (C8–C30+). Org. Geochem. 39, 284–288. https://doi.org/10.1016/j.orggeochem.2007.12.009.

Hayes, J.M., 2001. Fractionation of carbon and hydrogen isotopes in biosynthetic processes. Rev. Mineral. Geochem. 43, 225–277. https://doi.org/10.2138/gsrmg.43.1.225.

Hochuli, P.A., 1985. Palynostratigraphische Gliederung und Korrelation des Permokarbons der Nordschweiz. Eclogae Geol. Helv. 78, 719–831.

ICCP, 1998. The new vitrinite classification (ICCP System 1994). Fuel 77, 349–358. https://doi.org/10.1016/S0016-2361(98)80024-0.

ICCP, 2001. The new inertinite classification (ICCP System 1994). Fuel 80, 459–471. https://doi.org/10.1016/S0016-2361(00) 00102-2.

Jenkyns, H.C., 1985. The early Toarcian and Cenomanian-Turonian anoxic events in Europe: comparisons and contrasts. Geol. Rundsch. 74, 505–518.

Kotarba, M.J., Clayton, J.L., 2003. A stable carbon isotope and biological marker study of Polish bituminous coals and carbonaceous shales. Int. J. Coal Geol. 55, 73–94.

Küspert, W., 1982. Environmental change during oil shale deposition as deduced from stable isotope ratios. In: Einsele, S., Seilacher, A. (Eds.), Cyclic and Event Stratification. Springer, New York, pp. 482–501.

Laggoun-Défarge, F., Bourdon, S., Chenu, C., Défarge, C., Disnar, J.R., 1999. Etude des transformations morphologiques précoces des tissus végétaux dans la tourbe du marécage de Tritrivakely (Madagascar). Apports des techniques de marquage histochimique en MET et du cryo-MEB haute résolution. In: Elsass, V.F., Jaunet, A.-M. (Eds.), Structure et Ultrastructure des Sols et des Organismes, Les Colloques No. 92. INRA, Versailles, pp. 169–182.

Lahusen, P.H., Wyss, R., 1995. Erdöl- und Erdgasexploration in der Schweiz: ein Rückblick. Bullet. Assoc. Suisse Geol. Ingnieurs Petrol. 62, 43–72.

Langford, F.F., Blanc-Valleron, M.-M., 1990. Interpreting Rock–Eval pyrolysis data using graphs of pyrolyzable hydrocarbons vs. total organic carbon. AAPG (Am. Assoc. Pet. Geol.) Bull. 74, 799–804.

Laubscher, H., 1987. Die tektonische entwicklung der Nordschweiz. Eclogae Geol. Helv. 80, 287–303.

Leu, W., 2008. Permokarbon-Kartenskizze (Rohstoffe) Kompilation eines GIS-Datensatzes auf der Basis von bestehenden Unterlagen (Bereich Schweizer Mittelland). NAGRA. Arbeitsbericht NAB 08-49.

Leu, W., Greber, E., Schegg, R., 2001. Basin modeling NE-Switzerland, burial, erosion and temperature history of wells Benken, Weiach and Herdern-1. Unpubl. Nagra Int. Rep.

Leu, W., 2014. Potenzial der Kohlenwasserstoff Ressourcen in der Nordschweiz. NAB 14-70 NAGRA.

Leu, W., 2012. Swiss oil/gas exploration and lessons learnt. Swiss Bull. Angew. Geol. 17, 49–59.

Littke, R., Rotzal, H., Leythaeuser, D., Baker, D.R., 1991. Lower Toarcian Posidonia shale in Southern Germany (Schwaebische Alb). Organic facies, depositional environment and maturity. Erdöl Kohle Erdgas Petrochem. Hydrocarbon Technol. 44, 407–414.

Mackenzie, A.S., Maxwell, J.R., 1981. Assessment of thermal maturation in sedimentary rocks by molecular measurements. In: Brooks, J. (Ed.), Organic Maturation Studies and Fossil Fuel Exploration. Academic Press, London, p. 239e254.

Madritsch, H., Naef, H., Meier, B., Franzke, H.J., Schreurs, G., 2018. Architecture and kinematics of the Constance-Frick Trough (northern Switzerland): implications for the formation of post-Variscan basins in the foreland of the Alps and scenarios of their Neogene reactivation. Tectonics 37. https://doi.org/10.1029/2017TC004945.

Matter, A., 1987. Faciesanalyse und Ablagerungsmilieu des Permokarbons im Nordschweizer Trog. In: Eclogae Geologicae Helvetiae, Band, 80, Heft 2.

Matter, A., Peters, T., Bläsi, H.-R., Meyer, J., Ischi, H., Meyer, C., 1988. Sondierbohrung Weiach – geologie. Text- und Beilagenband. In: Nagra Tech. Ber. NTB 86–01. Nagra, Wettingen.

Mazurek, M., Hurford, A.J., Leu, W., 2006. Unravelling the multi-stage burial history of the Swiss Molasse Basin: integration of apatite fission track, vitrinite reflectance and biomarker isomerisation analysis. Basin Res. 18, 27–50, 2006.

McArthur, A.D., Kneller, B.C., Wakefield, M.I., Souza, P.A., Kuchle, J., 2016. Palynofacies classification of the depositional elements of confined turbidite systems: examples from the Gres d'Annot, SE France. Mar. Petrol. Geol. 77, 1254–1273.

McCann, T., Pascal, C., Timmerman, M.J., Krzywiec, P., López-Gómez, J., Wetzel, A., Krawczyk, C.M., Rieke, H., Lamarch, J., 2006. Post-variscian (end Carboniferous – early permian) basin evolution in western and central Europe. In: Gee, D.G., Stephenson, R.A. (Eds.), European Lithosphere Dynamics. Geological Society, London, pp. 355–388.

Mercuzot, M., Bourquin, S., Pellenard, P., Beccaletto, L., Schnyder, J., Baudin, F., Ducassou, C., Garel, S., Gand, G., 2022. Reconsidering Carboniferous–Permian continental paleoenvironments in eastern equatorial Pangea: facies and sequence

stratigraphy investigations in the Autun Basin (France). Int. J. Earth Sci. 111, 1663–1696. https://doi.org/10.1007/s00531-022-02200-6.
Mercuzot, M., Thomazo, C.S., Schnyder, J., Pellenard, P., Baudin, F., Pierson-Wickmann, A.-C., Sans-Jofre, P., Bourquin, S., Beccaletto, L., Santoni, A.-L., Gand, G., Buisson, M., Glé, L., Muiner, T., Saloume, A., Boussaid, M., Boucher, T., 2021. Carbon and nitrogen cycle dynamic in continental late-Carboniferous to early permian basins of eastern Pangea (Northeastern Massif central, France). Front. Earth Sci. 9, 705351. https://10.3389/feart.2021.705351.
Misch, D., Leu, W., Sachsenhofer, R.F., Gratzer, R., Rupprecht, B., Bechtel, A., 2017. Shallow hydrocarbon indications along the Alpine thrust belt and adjacent foreland basin: distribution and implications for petroleum exploration. J. Petrol. Geol. 40 (4), 341–362.
Moldowan, J.M., Dahl, J., Huizinga, B.J., Fago, F.J., Hickey, L.J., Peakman, T.M., Taylor, D.W., 1994. The molecular fossil record of oleanane and its relation to angiosperms. Science 265, 768–771.
Moscariello, A., 2019. Exploring for geo-energy resources in the Geneva Basin (Western Switzerland): opportunities and challenges. Swiss Bull. Angew. Geol. 24/2, 105–124.
Moscariello, A., Guglielmetti, L., Omodeo-Salé, S., De Haller, A., Eruteya, O.E., Lo, H.Y., Clerc, N., Makloufhi, Y., Do Couto, D., Ferreira De Oliveira, G., Perozzi, L., Hollmuller, P., Quiquerez, L., Nawratil De Bono, C., Martin, F., Meyer, M., 2020. Heat production and storage in Western Switzerland: advances and challenges of intense multidisciplinary geothermal exploration activities, an 8 years progress report. In: Proceedings World Geothermal Congress. Reykjavik, Iceland.
Moscariello, A., Ventra, D., Cervelli, M., Eruteya, O.E., Omodeo Salé, S., Makhloufi, Y., 2021. Revisiting the Origin of the Carboniferous Infill of Swiss Post-hercynian Throughs: Insights from the Weiach-1 Borehole (Northern Switzerland). Extended Abstract 19th Swiss Geoscience Meeting, Geneva. Symposium 7: Stratigraphy and Sedimentology: processes and deposits through time. https://geoscience-meeting.ch/sgm2021.
NAGRA, 2002. Technischer Bericht - projekt Opalinuston: Konzept für die Anlagen und den Betrieb eines geologischen Tiefenlagers. Entsorgungsnachweis für abgebrannte Brennelemente, verglaste hochaktive sowie langlebige mittelaktive Abfälle. Nagra Tech. Ber. NTB, 02-02.
Noble, R.A., Alexander, R., Kagi, R.I., Knox, J., 1986. Identification of some diterpenoid hydrocarbons in petroleum. Org. Geochem. 10, 825–829.
Omodeo-Salé, S., Eruteya, O.E., Cassola, T., Baniasad, A., Moscariello, A., 2020. A basin thermal modelling approach to mitigate geothermal energy exploration risks: the St. Gallen case study (eastern Switzerland). Geothermics 87, 101876.
Omodeo-Salé, S., Hamidi, Y., Villagomez, D., Moscariello, A., 2021. Quantifying multiple erosion events in the distal sector of the northern Alpine Foreland Basin (North-Eastern Switzerland), by combining basin thermal modelling with vitrinite reflectance and apatite fission Tract. Geosciences 11, 62. https://doi.org/10.3390/geosciences11020062.
Peters, K.E., Walters, C.C., Moldwan, J.M., 2005. The Biomarker Guide, second ed. Cambridge University Press, Cambridge, UK.
Peters-Kottig, W., Strauss, H., Kerp, H., 2006. The land plant $\delta^{13}C$ record and plant evolution in the Late Palaeozoic. Palaeogeogr. Palaeoclimatol. Palaeoecol. 240, 237–252. https://doi.org/10.1016/j.palaeo.2006.03.051.
Pickel, W., Kus, J., Flores, D., Kalaitzidis, S., Christanis, K., Cardott, B.J., Misz-Kennan, M., Rodrigues, S., Hentschel, A., Hamor-Vido, M., Crosdale, P., Wagner, N.I. C.C.P., 2017. Classifcation of liptinite– ICCP system (1994). Int. J. Coal Geol. 169, 40–61. https://doi.org/10.1016/j.coal.2016.11.004.
Pullan, C.P., Berry, M., 2019. A Paleozoic-sourced oil play in the Jura of France and Switzerland. Geol. Soc. Lond. Spec. Publ. 471 (1), 365–387. https://doi.org/10.1144/sp471.2.
Radke, M., 1988. Application of aromatic compounds as maturity indicators in source rocks and crude oils. Mar. Petrol. Geol.
Radke, M., Schaefer, R.G., Leythaeuser, D., Teichmüller, M., 1980. Composition of soluble organic matter in coals: relation to rank and liptinite fluorescence. Geochem. Cosmochim. Acta 44, 1787–1800.
Radke, M., Welte, D.H., Willsch, H., 1986. Maturity parameters based on aromatic hydrocarbons: influence of the organic matter type. Org. Geochem. 10, 51–63.
Radke D.H., M.Welte, 1983. The Methylphenanthrene Index (MPI): a maturity parameter based on aromatic hydrocarbons. In: Bjoroy, M. (Ed.), Advances in Organic Geochemistry 1981. Wiley, Chichester, pp. 504–512.
Sachsenhofer, R.F., Schulz, H.-M., 2006. Architecture of Lower Oligocene source rocks in the Alpine Foreland Basin: a model for syn- and postdepositional source rock features in the Paratethyan Realm. Petrol. Geosci. 12, 363–377.
Sachsenhofer, R.F., Leitner, B., Linzer, H.-G., Bechtel, A., Ćorić, S., Gratzer, R., Reischenbacher, D., Soliman, A., 2010. Deposition, erosion and hydrocarbon source potential of the Oligocene eggerding formation (Molasse basin, Austria). Aust. J. Earth Sci. 103, 76–99.
Schnyder, J., Stetten, E., Baudin, F., Pruski, A.-M., Martinez, P., 2017. Palynofacies reveal fresh terrestrial organic matter inputs in the terminal lobes of the Congo Deep-Sea fan. Deep-Sea Res. II 142, 91–108.
Schouten, S., Klein Breteler, W.C.M., Blokker, P., Schogt, N., Rijpstra, W.I.C., Grice, K., Baas, M., Sinninghe Damsté, J.S., 1998. Biosynthetic effects on the stable carbon isotopic compositions of algal lipids: implications for deciphering the carbon isotopic biomarker record. Geochem. Cosmochim. Acta 62, 1397–1406. https://doi.org/10.1016/S0016-7037(98)00076-3.
Schulz, H.-M., Sachsenhofer, R.F., Bechtel, A., Polesny, H., Wagner, L., 2002. The origin of hydrocarbon source rocks in the Austrian Molasse Basin (Eocene-Oligocene transition). Mar. Petrol. Geol. 19, 683–709.
Sebag, D., Copard, Y., Di Giovanni, C., Durand, A., Laignel, B., Ogier, S., Lallier-Verges, E., 2006. Palynofacies as useful tool to study origins and transfers of particulate organic matter in recent terrestrial environments: synopsis and prospects. Earth Sci. Rev. 79, 241–259.
Steffen, D., Gorin, G., 1993. Sedimentology of organic matter in Upper Tithonian-Berriasian deep-sea carbonates of southeast France: evidence of eustatic control. In: Katz, B., Pratt, L. (Eds.), Source Rocks in a Sequence Stratigraphic Framework: AAPG Studies in Geology, vol. 37, pp. 49–65.
Storme, J.-Y., Devleeschouwer, X., Schnyder, J., Cambier, G., Baceta, J.I., Pujalte, V., Di Matteo, A., Iacumin, P., Yans, J., 2012. The Palaeocene/Eocene boundary section at Zumaia (Basque-Cantabric Basin) revisited: new insights from high-resolution magnetic susceptibility and carbon isotope chemostratigraphy on organic matter (δ13Corg). Terra Nova 24, 310–317. https://doi.org/10.1111/j.1365-3121.2012.01064.x.
Sykes, R., Snowdon, L.R., 2002. Guidelines for assessing the petroleum potential of coaly source rocks using Rock-Eva pyrolysis. Org. Geochem. 33, 1441–1445.
Taylor, G., Teichmüller, M., Davies, A., Diessel, D., Littke, R., Robert, P., 1998. Organic Petrology: A New Handbook Incorporation Some Revised Parts of Stach's Textbook of Coal Petrology. Gebrüder Borntraeger, Berlin.
Thury, M., Gautschi, A., Mazurek, M., Müller, W., Naef, H., Pearson, F., Vomvoris, S., Wilson, W., 1994. Geology and hydrogeology of the crystalline basement of Northern Switzerland. Nagra Tech. Ber. NTB 93–01, 93, 01.
Tyson, R.V., 1995. Sedimentary organic matter. In: Organic Facies and Palynofacies.
Veron, J., 2005. The Alpine Molasse basin – review of petroleum Geology and remaining potential. Bull. Angew Geol. 10, 75–86.
Vollmayr, T., Wendt, A., 1987. Die Erdgasbohrung Entlebuch 1, ein Tiefenaufschluss am Alpennordrand. Bulletin der Vereinigung Schweiz. Petrol.-Geol. -Ingenieure 53, 67–79.
Wehner, H., Kuckelkorn, K., 1995. Zur Herkunft der Erdöle im nördlichen Alpen-Karpatenvorland. Erdol ErdGas Kohle 111, 508e514.
Wolf, M., Hagemann, W.H., Haverkamp, S., Linnenberg, W., 1988. Kohlenpetrographie und - chemie. In: Matter, A., et al. (Eds.), Sondierbohrung Weiach Geologic - Nagra Technischer Bericht NTB 86-01. Nagra, Baden, pp. 231–256.
Zdravkov, A., Bechtel, A., Sachsenhofer, R.F., Kortenski, J., 2017. Palaeoenvironmental implications of coal formation in Dobrudzha Basin, Bulgaria: insights from organic petrological and geochemical properties. Int. J. Coal Geol. 180, 1–17.
Ziegler, P.A., Schumacher, M.E., Dezes, P., van Wees, J.D., Cloetingh, S., 2006. Post-variscan evolution of the lithosphere in the area of the European Cenozoic rift system. In: Gee, D.G., Stephenson, R.A. (Eds.), European Lithospheric Dynamics, vol. 32. Geological Society, London, Memoirs, pp. 97–112.